

**A Review and Comparison of Pulse Width Modulation (PWM) Methods
For Analog and Digital Input Switching Power Amplifiers**

Preprint 4446 (G4)

Karsten Nielsen
Bang & Olufsen, Denmark
Institute of Automation, Technical University of Denmark

**Presented at
the 102nd Convention
1997 March 22–25
Munich, Germany**



AES

This preprint has been reproduced from the author's advance manuscript, without editing, corrections or consideration by the Review Board. The AES takes no responsibility for the contents.

Additional preprints may be obtained by sending request and remittance to the Audio Engineering Society, 60 East 42nd St., New York, New York 10165-2520, USA.

All rights reserved. Reproduction of this preprint, or any portion thereof, is not permitted without direct permission from the Journal of the Audio Engineering Society.

AN AUDIO ENGINEERING SOCIETY PREPRINT

A Review and Comparison of Pulse Width Modulation (PWM) methods for analog and digital input switching power amplifiers

Karsten Nielsen

Bang & Olufsen A/S, Denmark
and

Institute of Automation, Technical University of Denmark

E-mail: kn@iau.dtu.dk

Internet: <http://www.iau.dtu.dk/~kn>

Abstract

Switching power amplifiers can be based on numerous different and rather complicated non-linear modulation methods. This work is an attempt to review and compare a complete collection of 12 pulse width modulation methods, of which several have not been considered before. There is a lack of such fundamental reference material, and it is thought that further development in the field can result from a more fundamental and in-depth understanding of the principles involved. All major modulations classes: natural sampled PWM (NPWM), uniform sampled PWM (UPWM) and hybrid sampling schemes are analyzed and compared by analytical means and by simulation. A new efficient analysis tool, the Harmonic Envelope Surface (HES) is introduced to aid in the deep understanding of the modulation processes. Detailed measurements for an implemented amplifier example are given, to illustrate the possibilities for high end audio specifications by high efficiency switching power amplification.

1. Introduction

Recent research activity has shown that switching power amplification is likely to be an area with considerable possibilities in the near future, due to the unique combination of high efficiency, high fidelity and low complexity that has been proved obtainable in recent publications [29], [30]. A central element in a such a system is the pulse modulator to synthesize the train of pulses. This element can be based on numerous different analog or digital implemented non-linear modulation methods. This work attempts to provide an in-depth study and comparison of *all* possible pulse width modulation schemes, that can be realized in principle with a maximum of 4 independently controlled switches. Previous work in the field of pulse width modulation as e.g. in [2], [3], [5], [6], [9], [11], [13], [15], [16], [22] has concentrated on a limited set of modulation schemes and/or other applications than switching power amplification, where the objectives may be very different. The trend in recent years has been to

investigate a digital implementation of the modulator. This paper does *not* follow this trend, but attempts to step back and consider the modulator a general element, where the quality of the *output* and the modulator complexity is considered of primary importance, and the practical method and domain of implementation of minor importance.

To the best of the author's knowledge, no work exists which analyses and compares *all* modulation schemes that can be synthesized by four independently controlled switches with focus on switching power amplification as a specific application. Further motivating factors for reviewing and comparing pulse width modulation schemes are :

- Interesting characteristics of the more known modulation schemes have not drawn sufficient attention.
- Some fundamental modulation schemes have not been analyzed at all, although they may have advantageous characteristics.

All major modulations classes are analyzed and compared: natural sampled PWM (NPWM), uniform sampled PWM (UPWM) and hybrid sampling methods with focus on linearized PWM (LPWM) [24].

2. Pulse modulation based power amplification

The basic elements of a pulse modulation based power amplifier are illustrated in Fig. 1. The four general blocks are the pulse modulator, the switching power stage, the passive demodulation filter and error correction circuitry. The four essential blocks are discussed in general terms in the following.

2.1 The pulse modulator

The general pulse modulator outputs a train of pulses, which has a general spectral content as illustrated in Fig. 2. The modulator output generally contains three distinct elements:

- The input signal component (sine input assumed in Fig. 2).
- Distortion components of the input signal.
- A high frequency (HF) spectrum composed of either discrete components related to the carrier frequency and input signal, noise shaped noise or a combination of both.

The desired pulse modulator characteristics are :

- A high basic linearity, in order to minimize the need for error correction.
- A minimal switching frequency (f_s) / bandwidth (B) ratio.
- A minimum of HF spectral content at all modulation depths. The ideal modulator would generate *no* HF-components. An interesting new modulation method/modulator topology where this is theoretically possible is presented in the parallel paper [31].

- A low modulator complexity for easy implementation.

The pulse modulator can be based on pulse width modulation (PWM) or pulse density modulation (PDM). Since PDM is a quantizing pulse modulation scheme, the HF spectrum has a stochastic nature. Some reports have been given on the use of PDM both in a digital modulator implementation and analog implementation with the power stage incorporated in the loop [19], [28]. However, the average switching frequency is higher than that obtainable with PWM. This leads to lower performance and a considerably lower efficiency compared with e.g. the PWM based topologies recently presented in [29], [30]. A further disadvantage is the necessity for a high order loop filter in order to obtain a sufficient noise shaping effect. This is difficult to realize and limits the modulation depth of the modulator. Consequently, PDM is not considered to be a suitable modulation scheme for pulse modulated power amplifier systems, and will not be considered further.

2.2 The power switch

The power switch converts the incoming small-signal pulse modulated waveform to power levels. High efficiency is obtained by the on/off operation of the power transistors, i.e. they do in principle never enter the active region. An attractive realization of the power switch is the bridge topology, shown in Fig. 4. The topology can realize all of the considered modulation schemes in this paper. Some of the modulation schemes can be realized with a simpler half bridge, and this should be considered in their favour.

2.3 The demodulation filter

The demodulation filter is realized as a passive filter. The filtering requirements will depend on the modulation scheme, and of course the requirements on the output. In general though, the demands can be realized by two basic topologies:

- Differential + common-mode filtering topology, as illustrated in Fig. 4 (a second order filter).
- The simpler pure differential filtering topology, with no references to ground (other than HF). This simpler filter realization is possible if the modulation scheme produces no common-mode components on the bridge terminals.

The pure differential realization requires four times less (typically high quality) capacitance. Furthermore, the differential filter topology is effectively implemented by using double wound cores which halves the number of inductors, and reduces the total copper volume. So, common-mode filtering requirements seriously influence the demodulation filter complexity.

2.4 Error correction

Error correction is the general term for compensation schemes for the inevitable errors that will be introduced in each of the three forward path

blocks. This may be implemented by single or multiple-loop linear feedback [8], [26], [29], [30], feedforward [7] or even non-linear feedback [23]. Linear feedback topologies have proven to implement superior performance in the recent publications [29], [30]. Further steps towards high end switching power amplification are taken in this paper by combining attractive modulation schemes with powerful feedback control schemes. The results are given in section 9.

Numerous attempts have been made to implement the open loop topology (mainly based on digital PWM) without compensation for modulator errors, power stage errors and post filter errors [11], [14], [15], [16], [17], [21], [22]. The fact that *no* amplifiers have been built with a reasonable power handling capability and reasonable audio specifications, shows that this approach has failed. The causes are mainly the numerous non-ideal characteristics bound to the principle:

1. Any modulator and power switch non-linearity errors are fed directly to the load. Correlated errors introduce distortion and non-correlated errors introduce noise.
2. There is no rejection of power supply perturbations. Since the power stage output is largely proportional with the supply voltage, any supply ripple will intermodulate with the audio signal. In other words, $PSRR=0\text{dB}$.
3. The total amplifier output impedance is high due to the finite switch impedance and the filter impedance.
4. The sensitivity to load variations is high due to the passive demodulation filter. Accordingly, changes in load impedance will distort the frequency response of the amplifier.
5. The sensitivity to temperature drift, component tolerances and aging effects is high. The non-controlled switching amplifier is therefore not robust.

By applying efficient error correction, dramatically improved and much more consistent performance can be obtained. Furthermore, the need for costly tuning procedures etc. is eliminated, and the total cost of the system will in general be reduced.

3. Pulse width modulation schemes

Traditionally, pulse width modulation is categorized in two major classes by the sampling method: natural sampled PWM (NPWM) and uniform sampled PWM (UPWM). Alternative sampling methods exists [3], [12], [14] which can be categorized as hybrid sampling methods since the nature of sampling lies between the natural and uniform sampling. The principles of the different sampling methods is illustrated in Fig. 3. Several variants of these three basic modulation variants can be defined, and Table 1 shows the considered variants. The hierarchical structure illustrates the order in which the modulation schemes

Sampling method	Edge	Levels	Abbreviation
Natural sampling (NPWM)	Single sided	Two (AD)	NADS
		Three (BD)	NBDS
	Double sided	Two (AD)	NADD
		Three (BD)	NBDD
Uniform sampling (UPWM)	Single sided	Two (AD)	UADS
		Three (BD)	UBDS
	Double sided	Two (AD)	UADD
		Three (BD)	UBDD
Hybrid sampling (LPWM)	Single sided	Two (AD)	LADS
		Three (BD)	LBDS
	Double sided	Two (AD)	LADD
		Three (BD)	LBDD

Table 1 The considered variants of pulse width modulation.

are differentiated. To systematically differentiate between the modulation variants, the following abbreviation method is defined:

$$\{\text{Sampling Method}\}\{\text{Switching}\}\{\text{Edge}\}$$

An example is NADS for Natural sampling - **AD** switching - Single sided modulation. Fig. 7 - Fig.14 illustrates the essential time domain waveforms for the considered 8 variants of natural and uniform sampling. The figures illustrate from top to bottom the modulating signal and carrier, the signal waveforms on each of the bridge phases and the differential- and common-mode output signals, respectively. The uniform pulse width modulation is based on comparison between the carrier and a sampled version of the signal. By using a triangle as reference, double sided modulation results. This modulation of both edges doubles the information stored in the resulting pulse train, although the pulse train frequency is same. Class AD and BD are the (somewhat misleading but standardized) abbreviations for two level and three level switching, as introduced in [4], and efficient synthesis of a three-level switching pulse train is illustrated in the time domain figures for NBDS, NBDD, UBDS and UBDD. Examples of NPWM and UPWM modulator implementation are given in Fig. 5.

The harmonic distortion present in uniform sampled PWM has led to alternative hybrid sampling schemes. In general the principle of linearizing UPWM has attracted some attention in recent years and variants exist [11], [12], [14], [15], [20], [21], [22], [24], [25]. One approach is interpolation of the sampled data to approach the characteristics of natural sampling as first introduced in [3], [13], [14]. Linearized PWM (LPWM) [17], [24] is chosen in this work for comparison with UPWM and NPWM due to its simple implementation. The principle of hybrid sampled PWM by LPWM illustrated in Fig. 3. Note, how the LPWM waveform is much closer to the NPWM pulse waveform. A parameter

for optimization is the number of samples s used in each carrier cycle to approximate the input ($s = 3$ in Fig. 3). Clearly, the approximation is improved with s , however the complexity of the modulator also increases with s .

Fig. 6 illustrates the essential blocks of an LPWM modulator in a full bandwidth amplifier application. The basic principles are well known, and will not be described in detail. The interpolation factor (here 8) is determined by s and noise shaping considerations. The linearizer unit outputs the pulse width for the oversampled input samples. The practical implementation of LPWM requires the use of noise shaping, in order to reduce the counter clock speed which defines the time resolution. The noise shaper outputs the requantized pulse widths (8 bits in Fig. 6), which are converted to a PWM waveform by digital counter and comparator hardware in the PWM unit.

4. Analysis methodology

The analysis and comparison of the different modulation schemes is based on PWM responses to single tone input. Analytical treatment of modulated multitone and noise signal is highly complicated, and investigations are therefore deemed to be carried out by computer simulation. Most important however, the response to single tone input provides nearly all interesting information about the modulation process, and the response to multitone and noise inputs can in general be well predicted from the response to tonal input. The tonal behavior is analyzed by the well known double Fourier series approach from communications theory [1]. The method has been applied to a few PWM variants by Black [2]. Further treatment of the subject has been given by Bowes [5], [6] and Mellor [13]. The treatment in the referenced and other publications have typically been limited to a smaller set of modulation schemes and/or other applications, where the objectives may be very different. In this paper, a complete set of analytical expressions for NPWM and UPWM is derived for the first time.

LPWM is analyzed on *exactly* same parameters as NPWM and UPWM, that is non-quantized PWM responses to tonal stimuli. Besides the pure harmonic distortion, an important factor in the LPWM modulator is that the quantization noise and noise shaped noise introduced is sufficiently small and does not dominate over the harmonic distortion. Computer simulation is used to analyze LPWM, since a general compact double Fourier series expansion has not been derived as with NPWM and UPWM. Although the modulation processes cannot be investigated at the same level with computer simulation as by concise analytical expressions, computer simulation can provide sufficient resolution for a detailed investigation of all the given LPWM variants in Table 1.

4.1 Methods of comparison

All modulation processes depend in a way of several parameters as the modulation index, signal frequency and carrier frequency which complicates a general analysis and comparison. Furthermore, the objectives for choosing a given modulation method will inherently depend on the application, and numerous parameters can influence the choice of modulation strategy, as the maximal power level, target bandwidth, complexity/cost considerations etc. Still, it is attempted to carry out a unified comparison by considering the following important issues:

Spectral characteristics :

A detailed investigation of the high frequency spectral characteristics is carried out for each modulation scheme. These characteristics of the modulation spectrum differ considerably between modulation principles.

The frequency ratio is defined as the ratio between signal angular frequency ω and carrier angular frequency ω_c :

$$q = \frac{\omega}{\omega_c} \quad (1)$$

The theoretical maximum for q is not determined by the Nyquist criteria, as with normal amplitude sampling. It is determined by considering the carrier and signal slew-rates. The resulting limitations depend on the choice of edge modulation as:

$$SR_S = \frac{\omega_c}{2\pi} \Rightarrow \omega \leq \frac{\omega_c}{2\pi} \quad (\text{Single sided modulation}) \quad (2)$$

$$SR_D = 2 \frac{\omega_c}{2\pi} = \frac{\omega_c}{\pi} \Rightarrow \omega \leq \frac{\omega_c}{\pi} \quad (\text{Double sided modulation}) \quad (3)$$

In general, the high frequency spectral characteristics will have determining influence on the maximal frequency ratio (the bandwidth limit of the modulation process). Practical considerations as easy demodulation will therefore put tighter constraints on the possible frequency ratios than the limits defined in (2) and (3).

Since the HF spectral characteristics depend in a complex way off the parameters such as M , ω , ω_c a new analysis tool, the **Harmonic Envelope Surface (HES)** is defined to aid in the understanding the modulation process. The HES provides a detailed insight in the spectral characteristics with a single compact figure. The basic idea is to visualize the amplitude spectrum vs. the

important parameters modulation index M and normalized frequency (f/f_s). Instead of a 3D visualization, a much better approach is to visualize the HES in 2D with color (grayscale) defining amplitude. The parameter space defining the HES-plots in this paper is:

- $M \in \{-100; 0\}$,
- $q = 1/16$
- $f \in \{0, 4\}$, where f is the normalized frequency (f/f_s).

The choice of frequency ratio is not of primary importance in order to reveal the characteristics and *differences* between modulation schemes. The results can easily be generalized to other frequencies. However, it is appropriate to choose a frequency ratio close to a worst case situation, which is the case with $q = 1/16$.

Distortion

Some of the modulation schemes generate ‘forward’ harmonic distortion and it is therefore valid to consider total harmonic distortion (THD) as a comparison parameter. THD is investigated vs. frequency ratio q in the worst case situation $M = 0\text{dB}$.

5. Analysis

In the following, a complete set of analytical double Fourier series expressions are derived. Several of the expressions, e.g. for NBDS and UBDS, have not previously been published in the literature, and the derivation will therefore be treated in greater detail. HES-plots are derived on the basis of the expressions, and the spectral characteristics and distortion characteristics are analyzed and compared.

5.1 Natural sampled - AD - Single sided modulation (NADS)

Fig. 7 illustrates interesting time domain signals for NADS. Either the leading or the trailing edge can be modulated in single sided modulation, however the amplitude spectrum is the same for both variants and there will be no differentiation between the two variants in the following discussion. Note from Fig. 7 that no common-mode components are present over the bridge phases. The following will show, that this is a general characteristic of the two level modulation process. In appendix A, the double Fourier series (DFS) expression for NADS is developed in detail, and the background for using a double Fourier series approach is discussed. The DFS for NADS is repeated below:

$$\begin{aligned}
F_{NADS}(t) = & M \cos(y) \\
& + 2 \sum_{m=1}^{\infty} \frac{1 - J_0(m\pi M) \cos(m\pi)}{m\pi} \sin(mx) \\
& - 2 \sum_{m=1}^{\infty} \sum_{n=\pm 1}^{\infty} \frac{J_n(m\pi M)}{m\pi} \sin(mx + ny - m\pi - \frac{n\pi}{2})
\end{aligned} \tag{4}$$

Where:

M	Modulation index. $M \in [0; 1]$.
$x = \omega_c t$	$\omega_c =$ Carrier signal angle frequency.
$y = \omega t$	$\omega =$ Audio signal angle frequency.
J_n	Bessel function of nth order.
n	Index to the harmonics of the audio signal.
m	Index to the harmonics of the carrier signal.

The individual components present in the output spectrum are identified to be:

Component	Amplitude
m'th harmonic of carrier my	$2 \frac{1 - J_0(m\pi M) \cos(m\pi)}{m\pi}$
IM-component $mx \pm ny$	$\frac{2J_n(m\pi M)}{m\pi}$

One of the most important conclusions from the expression for NADS is that the modulating signal is left unchanged by the modulation, i.e there are *no direct forward harmonics*. This means that the modulation process by appropriate filtering can be considered *ideal* in terms of distortion. This is a very pleasant general characteristic of natural sampling. Fig. 15 illustrates the spectral characteristics of the modulation process, by two single ‘shots’ at $M=0\text{dB}$ and $M=-40\text{dB}$, and by a Harmonic Envelope Surface (HES). From the hHES-plot, the following interesting facts are concluded for NADS:

- The intermodulation components are very pronounced at $mx \pm ny$, and depend heavily on the modulation index M . This is seen as ‘skirts’ around harmonics of the carrier.
- The components related to the *even* harmonics of the carrier reduce with M , and are totally eliminated at idle. At lower M , the dependency between the dominating IM-components and M is nearly linear due to the characteristics of the 1st order Bessel function $J_1(x)$ (Fig. A.2).

As mentioned above, $q = 1/16$ represents a close to worst case situation. At lower frequencies, the ‘skirts’ will close to the carrier, which is clearly more

attractive especially when considering the components placed below the first harmonic of the carrier. Higher frequency ratios would produce in-band IM-components and increase the requirements for demodulation.

5.2 Natural sampled - BD - Single sided modulation (NBDS)

To the best of the authors knowledge, a double Fourier series for Natural sampled BD Single sided modulation (NBDS) has not been derived in previous literature in the field. The interesting time domain signals of the NBDS modulation process are illustrated in Fig. 8. Note the presence of a high frequency common-mode signal at the bridge phases, which illustrates the necessity for common-mode filtering. The derivation of a double Fourier series for NBDS will be carried out in the following in some detail. The approach used in appendix A could equally be used to derive the double Fourier series for NBDS. A much simpler approach however is to devise the expression by simple superposition rules from the expression for NADS, since NBDS can be synthesized by a 180 degree phase shift of the modulating signal to the opposing half-bridge. Subsequently, what is needed is a general expression for NADS with a phase shifted modulating signal. This is found by simply replacing y with $y-\phi$ in (4):

$$\begin{aligned}
 F_{NADS,\phi}(t) &= M \cos(y - \phi) \\
 &+ 2 \sum_{m=1}^{\infty} \frac{1 - J_0(m\pi M) \cos(m\pi)}{m\pi} \sin(mx) \\
 &- 2 \sum_{m=1}^{\infty} \sum_{n=\pm 1}^{\infty} \frac{J_n(m\pi M)}{m\pi} \sin(mx + ny - m\pi - \frac{n\pi}{2} - n\phi)
 \end{aligned} \tag{5}$$

$F_{NBDS}(t)$ is defined as :

$$F_{NBDS}(t) = \frac{F_{NADS}(t) - F_{NADS,\pi}(t)}{2} \tag{6}$$

The scaling is necessary in order to obtain a total pulse amplitude of 2. From (5) and (6) we get:

$$\begin{aligned}
2F_{NBDS}(t) &= M \cos(y) - M \cos(y - \pi) \\
&+ 2 \sum_{m=1}^{\infty} \frac{1 - J_0(m\pi M) \cos(m\pi)}{m\pi} \sin(mx) \\
&- 2 \sum_{m=1}^{\infty} \frac{1 - J_0(m\pi M) \cos(m\pi)}{m\pi} \sin(mx) \\
&- 2 \sum_{m=1n=\pm 1}^{\infty} \sum_{n=1}^{\infty} \frac{J_n(m\pi M)}{m\pi} \sin(mx + ny - m\pi - \frac{n\pi}{2}) \\
&+ 2 \sum_{m=1n=\pm 1}^{\infty} \sum_{n=1}^{\infty} \frac{J_n(m\pi M)}{m\pi} \sin(mx + ny - m\pi - \frac{n\pi}{2} - n\pi)
\end{aligned} \tag{7}$$

⇕

$$\begin{aligned}
2F_{NBDS}(t) &= 2M \cos(y) \\
&+ 2 \sum_{m=1n=\pm 1}^{\infty} \sum_{n=1}^{\infty} \frac{J_n(m\pi M)}{m\pi} \cos(mx + ny - m\pi - \frac{n\pi}{2}) \\
&- 2 \sum_{m=1n=\pm 1}^{\infty} \sum_{n=1}^{\infty} \frac{J_n(m\pi M)}{m\pi} \cos(mx + ny - m\pi + \frac{n\pi}{2})
\end{aligned} \tag{8}$$

Since :

$$\sin(z - \frac{n\pi}{2}) = -\cos(z) \sin(\frac{n\pi}{2}) \quad \text{and} \quad \sin(z + \frac{n\pi}{2}) = \cos(z) \sin(\frac{n\pi}{2}) \tag{9}$$

we can reduce (8) to :

$$\begin{aligned}
F_{NBDS}(t) &= M \cos(y) \\
&- 2 \sum_{m=1n=\pm 1}^{\infty} \sum_{n=1}^{\infty} \frac{J_n(m\pi M)}{m\pi} \cos(mx + ny - m\pi) \sin(\frac{n\pi}{2})
\end{aligned} \tag{10}$$

The individual harmonic components are identified to be:

Component	Amplitude
IM component $mx \pm ny$	$\frac{2J_n(m\pi M)}{m\pi} \sin(\frac{n\pi}{2})$

Fig. 16 illustrates the general spectral characteristics for NBDS. By comparing NADS and NBDS HES-plots, several important differences are observed :

- The determining IM components $mx \pm ny$ are close to linearly ($J_1(x)$) dependent on the modulation index at lower output levels. The HES-surface shows very pleasant spectral characteristics at lower output levels, and all

high frequency components disappear at idle. This is a very important advantage of NBDS.

- Whereas all harmonics of the carrier were present in NADS (especially the odd harmonics), they are *not* present in NBDS at all.
- All IM-components $mx \pm ny$ with even n are *eliminated*, meaning that the spectrum only contains half the components compared to NADS. This causes the ‘striped’ nature of the HES-plot.
- The maximal IM-component amplitudes are lower than in NADS, as a consequence of the synthesis of three switching levels.

Based on the this clearly improved theoretical performance, NBDS is concluded to be superior in terms of modulation spectra in comparison to NADS.

5.3 Natural sampled - AD - Double sided modulation (NADD)

Fig. 9 illustrates the time domain waveforms for NADD. Obviously, NADD modulates both leading and trailing edges of the pulses by using a triangle shaped reference. The double Fourier series has been synthesized in the literature in [6]. A simpler approach is the direct derivation from NADS by simple superposition:

$$F_{NADD}(t) = F_{NADS}(t) + F_{NADS}(-t) \quad (11)$$

A prerequisite for the above simple addition is that the leading and trailing edge modulated waveforms do not overlap. This is obtained by a simple selection of parameters. Following, by trigonometric reduction mechanisms the series can be derived :

$$\begin{aligned} F_{NADD}(t) = & M \cos(y) \\ & + 2 \sum_{m=1}^{\infty} \frac{J_0(m\pi \frac{M}{2})}{\frac{m\pi}{2}} \sin(\frac{m\pi}{2}) \cos(mx) \\ & + 2 \sum_{m=1}^{\infty} \sum_{n=\pm 1}^{\infty} \frac{J_n(m\pi \frac{M}{2})}{\frac{m\pi}{2}} \sin(\frac{(m+n)\pi}{2}) \cos(mx + ny) \end{aligned} \quad (12)$$

The modulation spectrum is composed of the following components:

Component	Amplitude
m'th harmonic of carrier my	$\frac{2J_0(m\pi \frac{M}{2})}{\frac{m\pi}{2}} \sin(\frac{m\pi}{2})$
IM-component $mx \pm ny$	$\frac{2J_n(m\pi M)}{\frac{m\pi}{2}} \sin((m+n)\frac{\pi}{2})$

Fig. 17 illustrates the general spectral characteristics for NADD modulation. The following interesting facts are concluded for NADD:

- The argument to the Bessel functions is *halved* in comparison with both single sided modulation schemes NADS and NBDS. This is important since the ratio by which the IM components reduces thereby is increased considerably. This is of special importance around the first harmonic of the switching frequency.
- Only IM-components with $(m+n)$ *odd* are present in the spectrum, meaning that about half the HF spectrum is eliminated in comparison to NADS, i.e. a 'striped' HES-plot occurs.
- Similar to NADS, NADD does not have a pleasant spectrum at low M , since the odd harmonics of the carrier are present with maximal amplitude.

From the modulation spectral characteristics, NADD must be concluded to be superior to NADS, but not as attractive as NBDS mainly due to the characteristics at lower modulation index. The smaller 'skirts' of NADD doesn't offset the advantages of the total elimination of carrier components that happen at lower output levels in NBDS.

5.4 Natural sampled - BD - Double sided modulation (NBDD)

Fig. 10 illustrates the synthesis of the NBDD pulse modulated waveform. The differential output illustrates a doubling in the number of samples, i.e. NBDD provides two samples pr. switch period. The modulation spectrum for NBDD as been derived in [5] by an approach similar to the one given en appendix A. Consistent with the approach used above, the spectrum for NBDD can however also be derived by simple superposition rules as:

$$F_{NBDD}(t) = \frac{F_{NADD}(t) - F_{NADD,\pi}(t)}{2} \quad (13)$$

Where

$$\begin{aligned}
F_{NADD,\pi}(t) &= M \cos(y - \pi) \\
&+ 2 \sum_{m=1}^{\infty} \frac{J_0(m\pi \frac{M}{2})}{\frac{m\pi}{2}} \sin(\frac{m\pi}{2}) \cos(mx) \\
&+ 2 \sum_{m=1}^{\infty} \sum_{n=\pm 1}^{\infty} \frac{J_n(m\pi \frac{M}{2})}{\frac{m\pi}{2}} \sin(\frac{(m+n)\pi}{2}) \cos(mx + ny - n\pi)
\end{aligned} \tag{14}$$

Again, the scaling in (11) is necessary in order to obtain a pulse train with an amplitude of 2. The derivation follows the scheme for NBDS, and the resulting double Fourier series for NBDD can be written as :

$$\begin{aligned}
F_{NBDD}(t) &= M \cos(y) \\
&- 4 \sum_{m=1}^{\infty} \sum_{n=\pm 1}^{\infty} \frac{J_n(m\pi \frac{M}{2})}{m\pi} \sin(\frac{(m+n)\pi}{2}) \sin(\frac{n\pi}{2}) \sin((mx + ny) - \frac{n\pi}{2})
\end{aligned} \tag{15}$$

The individual components are identified to be:

Component	Amplitude
IM-component $mx \pm ny$	$\frac{4J_n\left(m\pi \frac{M}{2}\right)}{m\pi} \sin\left(\frac{(m+n)\pi}{2}\right) \sin\left(\frac{n\pi}{2}\right)$

Fig. 18 shows the spectral characteristics for NBDD. The above outlined advantages of NBDS over NADS also hold when comparing NBDD with NADD. Furthermore, there is one extremely important advantage by using NBDD:

- The effective sampling frequency is *doubled*, while the carrierfrequency (and thereby the switching losses) are retained.

Looking at the HES-plot for NBDD, it has by far the most attractive spectral characteristics. As with NBDS, a drawback is the common-mode content at the bridge output terminals as illustrated in the time domain plots in Fig. 10.

5.5 Summary for NPWM

The systematic analysis of NPWM given above have illustrated the differing spectral characteristics for the four variants. The most important conclusion of the analysis is that NPWM is totally free from ‘forward’ harmonic distortion. In terms of modulation quality, it is possible to rank the four modulation variants from ‘best’ to ‘worst’:

1. NBDD
2. NBDS
3. NADD
4. NADS

The HF-characteristics of NBDD combines three attractive features:

- An effective doubling of the sampling frequency, which is beneficial for demodulation and control system design.
- A total elimination of *all* components related to the carrier.
- A near linear relationship between M and IM-component amplitude at lower modulation indexes, which causes the idle spectrum to be totally free from components.

6. Uniform sampling

As it will be shown in the following UPWM has distinctly different characteristics in comparison to NPWM. Again, double Fourier series expressions (DFS) are synthesized for all UPWM variants, and HES-plots are derived on the basis of the expressions and the spectral characteristics are compared.

6.1 Uniform sampled - AD - Single sided modulation (UADS)

The double Fourier series for single sided modulation has been devised in the general case by Black [2]. The derivation for uniform sampling follows the same scheme as for natural sampling. For UADS (here trailing edge modulation) the expansion can be written:

$$\begin{aligned}
 F_{UADS}(t) = & - \sum_{n=1}^{\infty} \frac{J_n(n\pi M q)}{n\pi q} \sin\left(ny - n\pi q - \frac{n\pi}{2}\right) \\
 & + \sum_{m=1}^{\infty} \frac{1 - J_0(m\pi M) \cos(m\pi)}{m\pi} \\
 & - \sum_{m=1}^{\infty} \sum_{n=\pm 1}^{\pm \infty} \frac{J_n((nq + m)\pi M)}{(nq + m)\pi} \sin\left(ny + mx - \frac{n\pi}{2}\right)
 \end{aligned} \tag{16}$$

We have the following amplitudes of the individual harmonics:

Component	Amplitude
n'th harmonic of signal	$\frac{J_n(n\pi M q)}{n\pi q}$
m'th harmonic of carrier frequency	$\frac{1 - J_0(m\pi M) \cos(m\pi)}{m\pi}$
IM component $mx \pm ny$	$\frac{J_n((nq + m)\pi M)}{(nq + m)\pi}$

Fig. 19 illustrates the spectral characteristics of UADS. In comparison to natural sampling (NADS) several important differing characteristics are observed from the HES-plot:

- Phase and amplitude distortion of the fundamental, i.e. the modulating input signal is not found unchanged in the pulse waveform.
- The spectrum contains forward harmonics of the input. The HES-plot illustrates the severe dependency of M for these components. The distortion is clearly not acceptable, e.g. THD=-20dB at M=0dB.
- By comparing HES-plots for NADS and UADS it is obvious, that the IM components for uniform sampling are *lower* than for natural sampling.

However, the differences are insignificant compared with the above mentioned factors.

The severe distortion is the most worst obstacle for UADS, and this factor alone makes the modulation scheme unusable in general switching power amplifier applications.

6.2 Uniform sampled - AD - Single sided modulation (UBDS)

To the best of the authors knowledge, UBDS has not previously been treated in the literature, and the derivation of the series will therefore be treated in some detail in the following. Fig. 11 illustrates the time domain waveforms for UBDS. The general expression for UBDS is derived from UADS by superposition, similar to the approach used for natural sampling. The series for UADS with a phase shifted modulating signal is:

$$\begin{aligned}
 F_{UADS,\phi}(t) = & -\sum_{n=1}^{\infty} \frac{J_n(n\pi Mq)}{n\pi q} \sin\left(ny - n\pi q - \frac{n\pi}{2} - n\phi\right) \\
 & + \sum_{m=1}^{\infty} \frac{\sin(mx) - J_0(m\pi M) \sin(mx - m\pi)}{m\pi} \\
 & - \sum_{m=1}^{\infty} \sum_{n=\pm 1}^{\pm\infty} \frac{J_n((nq+m)\pi M)}{(nq+m)\pi} \sin(ny + mx - \frac{n\pi}{2} - n\phi)
 \end{aligned} \tag{17}$$

By definition, the Fourier series for double sided uniform BD is generated by combining (17) and (16) and amplitude scaling as :

$$F_{UBDS}(t) = \frac{F_{NADS}(t) - F_{NADS,\pi}(t)}{2} \tag{18}$$

This leads to:

$$\begin{aligned}
 2F_{UBDS}(t) = & -\sum_{n=1}^{\infty} \frac{J_n(n\pi Mq)}{n\pi q} \sin\left(ny - n\pi q - \frac{n\pi}{2}\right) \\
 & + \sum_{n=1}^{\infty} \frac{J_n(n\pi Mq)}{n\pi q} \sin\left(ny - n\pi q - \frac{n\pi}{2} - n\pi\right) \\
 & - \sum_{m=1}^{\infty} \sum_{n=\pm 1}^{\pm\infty} \frac{J_n((nq+m)\pi M)}{(nq+m)\pi} \sin\left(ny + mx - \frac{n\pi}{2}\right) \\
 & + \sum_{m=1}^{\infty} \sum_{n=\pm 1}^{\pm\infty} \frac{J_n((nq+m)\pi M)}{(nq+m)\pi} \sin\left(ny + mx - \frac{n\pi}{2} - n\pi\right)
 \end{aligned} \tag{19}$$

⇕

$$\begin{aligned}
F_{UBDS}(t) = & \sum_{n=1}^{\infty} \frac{J_n(n\pi Mq)}{n\pi q} \cos(ny - n\pi q) \sin\left(\frac{n\pi}{2}\right) \\
& + \sum_{m=1}^{\infty} \sum_{n=\pm 1}^{\pm\infty} \frac{J_n((nq + m)\pi M)}{(nq + m)\pi} \cos(ny + mx) \sin\left(\frac{n\pi}{2}\right)
\end{aligned} \tag{20}$$

The individual harmonic amplitudes are:

Component	Amplitude
n'th harmonic of signal	$\frac{J_n(n\pi Mq)}{n\pi q} \sin\left(\frac{n\pi}{2}\right)$
IM component $mx \pm ny$	$\frac{J_n((nq + m)\pi M)}{(nq + m)\pi} \sin\left(\frac{n\pi}{2}\right)$

Fig. 20 shows the spectral characteristics for UBDS. The following apparent conclusions for UBDS can be drawn from the HES-plot:

- In comparison to UADS *all even order* forward harmonics are canceled out. This improves the resulting THD, since the now dominating 3. harmonic is around -40dB at M=0dB.
- Similar to the natural sampling case half of the IM components are canceled compared to UADS. This is the reason for the 'striped' nature of the HES-plot.
- All harmonics of the carrier are removed, including the carrier itself.
- The residue is free from components.

As expected, many of the positive characteristics of NBDS at lower levels are also found for UBDS, since uniform sampling approaches natural sampling when the modulation index goes towards zero. The most interesting aspect of UBDS is the cancellation of even order forward harmonics which makes it usable at much higher frequency ratios than UADS. The frequency dependency of THD is investigated more closely in section 6.5.

6.3 Uniform sampled - AD - Double sided modulation (UADD)

Fig. 13 illustrates the time domain signals for UADD. The double Fourier series is derived from UADS as :

$$F_{UADD}(t) = F_{UADS}(t) + F_{UADS}(-t) \tag{21}$$

The Fourier series for UADD can be written :

$$\begin{aligned}
F_{UADD}(t) = & \sum_{n=1}^{\infty} \frac{J_n\left(n\pi \frac{M}{2} q\right)}{n\pi q} \sin\left((q+1)\frac{n\pi}{2}\right) \cos(ny) \\
& + \sum_{m=1}^{\infty} \frac{J_0\left(m\pi \frac{M}{2}\right)}{m\pi} \cos\left(\frac{m\pi}{2}\right) \cos(mx) \\
& + \sum_{m=1}^{\infty} \sum_{n=\pm 1}^{\pm \infty} \frac{J_n\left((nq+m)\frac{\pi M}{2}\right)}{(nq+m)\pi} \sin\left((m+n(1+q))\frac{\pi}{2}\right) \cos(ny+mx)
\end{aligned} \tag{22}$$

Form the DFS, the following amplitudes of the individual harmonics are obtained:

Component	Amplitude
n'th harmonic	$\frac{J_n\left(n\pi \frac{M}{2} q\right)}{n\pi q} \sin\left((q+1)\frac{n\pi}{2}\right)$
m'th harmonic of carrier	$\frac{J_0\left(m\pi \frac{M}{2}\right)}{m\pi} \cos\left(\frac{m\pi}{2}\right)$
IM component $mx \pm ny$	$\frac{J_n\left((nq+m)\frac{\pi M}{2}\right)}{(nq+m)\pi} \sin\left((m+n(1+q))\frac{\pi}{2}\right)$

Fig. 21 shows spectral plots and a HES-plot for UADD. The following specific characteristics deserve attention :

- All forward harmonics are present, but at considerably reduced amplitude compared to UADS (at $M=0\text{dB}$).
- All IM-components are present at full scale, i.e. the total cancellation of half of the harmonic spectrum is *not* present, as it is the case with the natural sampling counterpart NADD.

6.4 Uniform sampled - BD - Double sided modulation (UBDD)

The Fourier series for UBDD is derived form UADS as:

$$F_{UBDD}(t) = \frac{F_{UADD}(t) - F_{UADD,\pi}(t)}{2} \tag{23}$$

We get:

$$\begin{aligned}
F_{UBDD}(t) = & -4 \sum_{n=1}^{\infty} \frac{J_n\left(n\pi q \frac{M}{2}\right)}{n\pi q} \sin\left((q+1)\frac{n\pi}{2}\right) \sin\left(\frac{n\pi}{2}\right) \sin\left(ny - \frac{n\pi}{2}\right) \\
& - 4 \sum_{m=1}^{\infty} \sum_{n=\pm 1}^{\pm \infty} \frac{J_n\left((nq+m)\frac{\pi M}{2}\right)}{(nq+m)\pi} \sin\left((m+n(1+q))\frac{\pi}{2}\right) \sin\left(\frac{n\pi}{2}\right) \sin\left(ny + mx - \frac{n\pi}{2}\right)
\end{aligned} \tag{24}$$

We have the following amplitudes of the individual harmonics:

Component	Amplitude
n'th harmonic	$\frac{J_n\left(n\pi \frac{M}{2} q\right)}{n\pi q} \sin\left((q+1)\frac{n\pi}{2}\right) \sin\left(\frac{n\pi}{2}\right)$
IM component $mx \pm ny$	$\frac{J_n\left((nq+m)\frac{\pi M}{2}\right)}{(nq+m)\pi} \sin\left((m+n(1+q))\frac{\pi}{2}\right) \sin\left(n\frac{\pi}{2}\right)$

Fig. 22 illustrates the spectral characteristics for UBDD. From the HES-plot, the following facts on UBDD deserve attention :

- Although UBDD provides two samples per pulse, it can *not* be considered as a doubling of the sampling frequency. There are remarkably high components around odd harmonics of the carrier. As expected, they decrease with M where the uniform sampling approaches natural sampling.
- Apart from UADD, UBDD *does* eliminate half of the harmonic spectrum ('striped' nature of HES-plot).
- All harmonics of the carrier (and the carrier itself) are eliminated in the spectrum.

6.5 UPWM summary

The systematic analysis of UPWM illustrated the widely different characteristics regarding distortion and HF-characteristics. Fig. 23 illustrates THD vs. q for all four UPWM schemes. The table below summarizes the frequency ratio's corresponding to a THD of -70dB:

	UADS	UBDS	UADD	UBDD
q (THD=-70dB)	0.0006	0.009	0.012	0.019

Not even UBDD delivers acceptable distortion at reasonably high frequency ratio's. Still, the different modulation schemes can be ranked from 'best' to 'worst' in terms of distortion and HF spectral characteristics :

- UBDD
- UBDS

- UADD
- UADS

UBDD ‘wins’ by a combination of lowest distortion and best HF-spectral characteristics, although the win is not as clear as the dual natural sampling scheme NBDD.

7. Hybrid sampling schemes

The thorough analysis given above on uniform sampled PWM has illustrated one fundamental problem of this ‘digital’ modulation scheme - the harmonic distortion. No uniform sampling PWM scheme can implement a very good digital modulator. The first publication addressing hybrid sampling schemes was given back in 1967 by Mananov [3] who called it modulation of the third kind. Several alternative hybrid sampling schemes been presented in recent years, with PWM D/A-converters and switching power amplifiers as specific application, as e.g. [12], [13], [14], [15]. The basic idea is the same - by sampling ‘in between’ the natural and uniform case, the harmonic distortion can be reduced, especially if the sampling approaches natural sampling. The digital algorithms required for the approximation vary in complexity. Where as the LPWM algorithm (Fig. 3) [17] is rather simple to implement, the polynomial approximation [14] requires a curve fitting algorithm and a numerical algorithm to find the crossing point, e.g. Least Squares (LS) can be used for the curve fitting, and the Newton Raphson algorithm can be used to determine the crossing point. Since the performance differences between the simple LPWM and more complex algorithms is insignificant, LPWM is chosen for investigation and comparison with the UPWM and NPWM sampling schemes.

As it was the case for NPWM and UPWM, it is the first time that all hybrid sampled variants (LPWM variants in Table 1) are analyzed and compared. However, the double Fourier integrals that arrive from this sampling approach can not be solved analytically, and a simple expansion into a double Fourier series is therefore not directly possible.

The tonal behavior is therefore investigated by computer simulation. In general, only *a single period* of the input tone is modulated, since all distortion information and modulation components can be derived from this approach. In order to obtain sufficient resolution in the analysis, a very fine time resolution is needed for the PWM waveform. 14-16 bits of resolution in every switch cycle provides more than 100dB of spectral resolution, which is enough for the analysis and comparison with NPWM and UPWM. Distortion of lower modulation indexes can not be investigated, but since the focus is on worst-case situations this is not a severe limitation. The four modulation variants will be analyzed with the following parameters set:

- $q = 1/16$, exactly as for NPWM and UPWM. The spectral characteristics are investigated vs. the number of approximating samples s , $s \in \{1,2,3,5\}$, where $s = 1$ corresponds to uniform sampling (Fig. 3).
- THD vs. q for $M = 0\text{dB}$ for different levels of interpolation ($s \in \{2,3,5\}$.)

7.1 Linearized - AD - Single sided modulation (LADS).

Fig. 24 illustrates from top to bottom the amplitude spectrum for $s \in \{1,2,3,5\}$ with the above defined parameters. From these amplitude spectra, the following is concluded:

- A dramatic improvement in THD is observed for increasing s . Thus, the distortion is reduced 50dB from $s = 1$ to $s = 5$. THD = -68dB with a frequency ratio as low as $q = 1/16$.
- The HF characteristics change with s , i.e the IM-component amplitude increase with s . At $s = 5$ the characteristics are very close to NADS.

7.2 Linearized - BD - Single sided modulation (LBDS).

Fig. 25 illustrates the amplitude spectrum for $s \in \{1,2,3,5\}$. The following is concluded:

- The distortion remains odd harmonic at all s .
- The total improvement in distortion from $s = 1$ (uniform sampling) to $s = 5$ is around 30dB.
- The HF characteristics change with s , i.e the IM-component amplitude increase with s . At $s = 5$ the characteristics are very close to NBDS.

7.3 Linearized - AD - Double sided modulation (LADD).

Fig. 26 illustrates the amplitude spectrum for $s \in \{1,2,3,5\}$. The following is observed:

- The total improvement in distortion from $s = 1$ (uniform sampling) to $s = 5$ is around 30dB as for LBDS.
- There are interesting changes in the HF-characteristics as the approximation accuracy increases. Half of the IM-components drop out as s increases.

7.4 Linearized - BD - Double sided modulation (LBDD).

Fig. 27 illustrates the amplitude spectrum for $s \in \{1,2,3,5\}$. The following is concluded:

- The improvement in distortion from the uniform sampling case to $s = 5$ is around 20dB, i.e LBDD is not linearized as effectively as the other schemes.
- All of the components around odd harmonics of the carrier *disappear* as the approximation accuracy is increased. At $s = 3$ the components are totally eliminated and LBDD therefore has the same attractive HF-characteristics as NBDD.

7.5 LPWM summary

Fig. 28 - Fig. 31 illustrates THD vs. q for $s \in \{2,3,5\}$, for the four LPWM methods. It is interesting to notice, that THD is close to linearly dependent on q as it was the case with uniform sampling. The reason for the increased distortion at higher q for LADS and LBDS with 5 samples approximation is due to IM-components and not forward harmonics (THD is based on an RMS sum of the 2. to 5. harmonic). Similarly, the deviations from the linear characteristic at very low output levels is due to the simulation accuracy.

From Fig. 28 - Fig. 31, THD is given at exactly $q = 1/16$:

(THD, $q = 1/16$)	$s = 1$	$s = 2$	$s = 3$	$s = 5$
LADS	-20.1 dB	-46.2 dB	-55.9 dB	-68.3 dB
LBDS	-36.9 dB	-46.3 dB	-58.3 dB	-68.8 dB
LADD	-39.8 dB	-46.0 dB	-58.4 dB	-68.9 dB
LBDD	-49.0 dB	-58.2 dB	58.4 dB	-68.0 dB

In combination with the THD vs. q investigations in Fig. 28 to Fig. 31, this clearly shows that THD is very sensitive to the number of samples s used in the approximation.

Another remarkable conclusion from the investigations is that the differences in distortion between modulation schemes diminish in LPWM, as the approximation accuracy is increased. At $s = 5$ the distortion is thus -68dB, independent of the modulation scheme. The *nature* of the distortion however is not the same as shown from the spectral amplitude illustrations. A general and important conclusion though, is that it is possible to realize acceptable performance by digital implemented LPWM modulators with all the considered modulation schemes. Due to this interesting characteristic of LPWM, the choice of modulation scheme is based on HF-spectral characteristics. This also means that the ranking of the different modulation schemes is similar to the ranking of NPWM from 'best' to 'worst':

- LBDD
- LBDS
- LADD
- LADS

LBDD clearly has the most attractive HF-characteristics, if the approximation is sufficiently good.

8. Problematic issues with digital LPWM modulation

Although the analysis of NPWM, UPWM and LPWM has been carried out on the same parameters, digital modulator implementation is dramatically different from analog modulator implementation, as it is apparent from the modulator examples in Fig. 6. The noise shaping causes the HF-spectrum to be a combination of both discrete components and noise.

The general problematic issues regarding digital PWM based switching power amplification can be summarized to:

- The problems of applying error correction for power stage and demodulation filter error components. This is the most severe problem, since the power stage distortion is typically orders of magnitude higher than in a high performance digital LPWM modulator. So, an error correction system is crucial.
- The noise shaped noise, which has to be removed by the demodulation filter.
- The problems by implementing double sided modulation, where two parameters need to be noise shaped.
- The PWM counter speed, which tends to be high especially in full bandwidth systems.

The problems of implementing the digital PWM modulator vary with modulation scheme, i.e. single sided modulation is simpler to implement than double sided modulation (this is not the case in natural sampled systems). Considering these problematic issues at the fact that NPWM has shown ideal performance and is easy to implement with high quality, it is not easy to argue for digital implementation of the modulator.

9. Example implementation

Detailed results for a implemented amplifier example is given, in order to show that very convincing audio performance can be delivered from a switching power amplifier system. The example is based on analog PWM, more specifically NBDD. The major specifications are given in the Table 2.

The specifications are now discussed in greater detail:

- Fig.32 illustrates the power stage efficiency vs. output power at two different carrier frequencies 50KHz and 250KHz. The efficiency is seen to approach 92% and 96% at higher output powers, respectively.
- Fig 34 illustrate THD+N vs. output power for 100Hz, 1KHz and 10KHz. The harmonic residue at 1W/1KHz (Fig 33) illustrates the reason for the extremely low distortion: All harmonics are damped more than 95dB relative to the fundamental !. This is extremely good for such a high power system.

Cont. output power	200W
Peak output power	300W
Bandwidth (3 dB)	0Hz - 80KHz
Load impedance	4 / 8 / 16
Supply voltage (single)	70V
THD+N (20Hz→ f_{max} , 0mW→ Po_{max})	0.001%-0.05%
CCIF IMD	<0.005%
Residual noise 20Hz-22KHz (unw)	50 μ V RMS
Dynamic range (unw)	118dB
Maximal efficiency	92%

Table 2 Full bandwidth NBDD based amplifier

- Fig. 35 further documents the well distributed amplifier noise at idle. The total RMS sum (20Hz-20KHz) is 50 μ V, corresponding to an unweighted dynamic range of near 118dB.
- The switching amplifier system also possesses extremely low intermodulation distortion (IMD) as illustrated by the standardized CCIF measurement in Fig. 36. The IMD is below 0.005%.

10. Conclusions

A detailed and systematic comparison of a complete collection of 12 natural sampled, uniform sampled, and hybrid sampled PWM methods have been carried out. For the first time, a complete set of analytical expressions are provided for all variants of natural and uniform sampled PWM. A new analysis tool, the Harmonic Envelope Surface (HES), was defined on the basis of the DFS expressions, in order to be able to investigate the spectral characteristics in detail with a single illustration. Some essential conclusions from the systematic review of pulse width modulation for switching power amplifier systems are:

- High quality pulse width modulation can be realized in both the analog domain by NPWM schemes and in the digital domain with LPWM schemes. However, NPWM is the optimal modulation strategy, mainly due to a perfect reproduction of the modulating signal in the pulse modulated waveform. Several problematic issues regarding digital LPWM implementation only emphasizes the advantages of NPWM in switching power amplifier applications.
- The double sided three level analog schemes (NBDD) and (LBDD) provide several advantages, the most important being the effective doubling of sampling frequency and the perfect modulation spectrum at idle which is free from components. These advantages offset the increase in modulator complexity.

- With practical frequency ratios, LPWM can provide excellent approximation to natural sampling for *all* variants LADS/LADD/LBDS/LBDD. However, the necessary number of samples for high quality approximation varies with modulation method.

Practical results for a 200W NBDD based power amplifier example were given to illustrate the possibility of realizing high efficiency switching power amplifier systems with high end performance, using the technology of today. It is hoped, that the detailed study and evaluation of pulse width modulation methods will help to a better understanding of the modulation processes and their advantages and disadvantages.

This paper has only concentrated on the pulse modulator, i.e. one out of the four major parts of the switching power amplifier. In order to realize a high performance amplifier system, all other three elements also need great attention. A detailed analysis of the possible variants of power stage, demodulation filter and the control system (error correction system) was outside the scope of this paper. Future publications are planned on these highly interesting subjects.

11. Acknowledgments

The author is grateful to professor John Vanderkooy, University of Waterloo, Canada for his comments on this and the parallel paper [31]. Furthermore, the author wishes to thank Bang&Olufsen, the Danish Energy Agency and CETEC for their economic/technical support in the research project.

12. References

(Arranged after date of publication)

- [1] Bennett, W. R.
" New Results in the Calculation of Modulation Products "
Bell system Technical Journal. 1933. pp. 228-243.
- [2] Black, H.S.
Modulation Theory
Van Nostrand Company, 1953.
- [3] Mananov, V. V
"Single polarity pulse width modulation of the third kind "
Telecomm. Rad. Eng. 1967, 22, (2), pp. 67-70.
- [4] Martin, J.D.
Theoretical efficiencies of class D power amplifiers.
Proc. IEE, Vol. 117, No. 6, 1970
- [5] Bowes, S. R.
" New sinusoidal pulsewidth-modulated inverter "
Proc. IEE, Vol. 122, No. 11, November 1975
- [6] Bowes, S.R. *et al.*

- "Novel approach to the analysis and synthesis of modulation processes in power converters"
Proc. IEE, Vol. 122, No. 5, May 1975.
- [7] Vanderkooy, John. " Feedforward error correction in power amplifiers "
JAES. Vol. 28. Num. 1. 1980. pp. 2-16.
- [8] Attwood, B. E.
" Design Parameters Important for the Optimization of Very-High-Fidelity PWM (Class D) Audio Amplifiers "
JAES. Vol. 31. No. 11. Nov. 1983.
- [9] Sethuraman, S. K. *et al.*
" PWM: A survey of modulation strategies, their spectrum analysis and microprocessor implementation ".
1987 UPEC. pp. 1-5.
- [10] Waheed, M. A. *et al.*
"An intelligent single-chip microcontroller based power controller for realtime applications "
IEE International Conference On Control 88. Conf. publ. no. 285. April 1988, Oxford. pp. 489-493.
- [11] Goldberg, J.M.
"New Results in PWM for Digital Power Amplification"
89th AES Convention, Los Angeles, Sept. 1990. Preprint 2959
- [12] Leigh, S.P. *et al.*
" Distortion minimisation in Pulse Width Modulated Systems Using a Digital Sampling Process"
Electronic Letters, 2nd August 1990. p. 1310-1311
- [13] Mellor, P.H. *et al.*
"Reduction of spectral distortion in class D amplifiers by an enhanced pulse width modulation sampling process"
IEE-Proceedings-G. Vol. 138, No.4, Aug 1991. pp.441-448
- [14] Goldberg, J.M. *et al.*
" Pseudo-Natural Pulse Width Modulation For High Accuracy Digital-To-Analogue Conversion"
Electronic Letters, 1st August 1991. p. 1491-1492
- [15] Goldberg, J. M.
Signal Processing for High Resolution Pulse Width Modulation Based Digital-To-Analogue Conversion.
Ph.D thesis. Kings College, University of London. November 1992.
- [16] Hawksford, M.O.J.
"Dynamic Model-Based Linearization of Quantized Pulse-Width Modulation for Applications in Digital-to-Analogue Conversion and Digital Power Amplifier Systems"

- JAES. Vol.40. No.4. April 1992. pp. 235-252.
- [17] Shajaan, M.
Digital PWM-forstærker til aktivt højttalersystem.
M.Sc. Thesis (in Danish).
Electronics Institute, Tech. Uni. of Denmark. 1992.
- [18] Mellor, P.H. *et al.*
" Digital Sampling Process for Audio Class D Pulse Width Modulated Power Amplifiers" .
Electronic Letters. 2nd jan 1992. Vol.28. pp. 56-58.
- [19] Klugbauer, J. *et al.*
"A Sigma-Delta modulated Switching Power Amp "
92nd AES Convention. Preprint 3227. Vienna. 1992.
- [20] Craven, P.
" Toward the 24 bit DAC: Novel Noise-Shaping Topologies Incorporating Correction for the Nonlinearity in a PWM Output Stage "
JAES. Vol.41, No.5. 1993. pp. 291-313.
- [21] Hiorns, R.E.
"Power Digital to Analogue conversion using pulse width modulation and digital signal processing"
IEE Proceedings-G. Vol. 140. No.5, Oct 1993. pp. 329-338.
- [22] R.E. Hiorns
"Digital Signal Processing and Circuit Design for Pulse Width Modulating Digital to Analogue Conversion "
Ph.D thesis. Kings College, University of London. 1994.
- [23] Lai, Zheren *et al.*
"A New Extension of One-Cycle Control and Its application to Switching Power Amplifiers"
IEEE APEC' 95. pp. 826-831.
- [24] Shajaan, Mohammad *et al.*
"All digital Power Amplifier Based on Pulse Width Modulation"
96th Convention of the AES. Feb. 1994. Amsterdam. Preprint 3809.
- [25] Hawksford, M.O.J.
"Linearization of Multi-Level, Multi-Width Digital PWM with Applications in Digital-to-Analogue Conversion"
97th Convention of the AES, November 1994. San Francisco.
Preprint 3908.
- [26] Vanderkooy, John
"New concepts in Pulse Width Modulation "
97th Convention of the AES, November 1994. San Francisco.
Preprint 3886.
- [27] Lai, R. S. *et al*

" A PWM Method for Reduction of Switching Loss in a Full-Bridge Inverter".

IEEE Transactions on Power Electronics, Vol. 10, No. 3, May. 1995.

[28] Iwata, K.

" A High-Efficient Pulse-Density Modulation Audio Power Amplifier "
101st AES Convention. Los Angeles, California. Preprint 4328.

[29] Nielsen, Karsten

"High Fidelity PWM based Amplifier Concept for active speaker systems with a very Low Energy Consumption"

100th AES Convention. Copenhagen, May 1996. Preprint 4259.

[30] Anderskov N., Nielsen, K. Andersen, M.

"High Fidelity Pulse Width Modulation Amplifiers based on Novel Double Loop Feedback Techniques"

100th AES Convention. Copenhagen, May 1996. Preprint 4258.

[31] Nielsen, Karsten

" Parallel Phase Shifted Carrier Pulse Width Modulation (PSCPWM) - A novel approach to switching power amplifier design "

To be presented on the 102th AES Convention. Munich, March 1996.

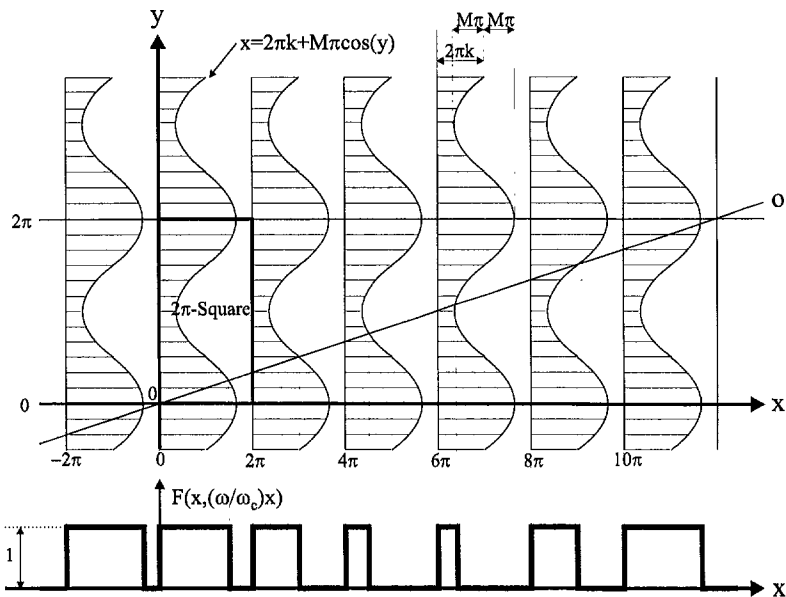


Figure A.1 Geometric surface to aid in the development of the double Fourier series.

13. Appendix A

The signal frequency and carrier are in general incommensurable, and the PWM waveform non-periodic. Thus, a double Fourier series expansion is necessary because, in the general case no relationship exists between the signal and the carrier. Bennett has used a 3-dimensional surface to analyze general "double periodic" waveforms. Fig. 1 illustrates a top view on the XOY-plane on this surface, defined as $F(x, y)$, here for the NADS modulation method.

The analysis is based on a sinusoidal input:

$$u(y) = 2\pi k + M\pi \cos(y) \quad (25)$$

The surface is defined by:

$$F(x, y) = \begin{cases} 1 & (x - |x|_{2\pi}) \leq u(y) \\ 0 & \text{otherwise} \end{cases} \quad (26)$$

where $|x|_{2\pi}$ is the closed multiple of 2π , which is less than x . The pulse width modulated wave can be synthesized from $F(x, y)$ by a plane perpendicular to the XOY-plane along the line OA, i.e by the ZOA-plane. This is done by projecting the *intersections* of the ZOA-plane with $F(x, y)$ onto the XOZ-plane. This projection is also illustrated in the bottom of Fig. 1.

By relating x and y to time as:

$$\begin{aligned} x &= \omega_c t \\ y &= \omega t \end{aligned} \quad (27)$$

Each value of time corresponds to a point on the OA-line in Fig. A.1. Note, that it is the exact shape of the contour that defines the type of sampling used. Natural sampling is synthesized by a straight line, while uniform sampling could be synthesized by a staircase waveform as illustrated in Fig. A.1.

The fundamental idea behind the 3-dimensional representation is seen by considering by XOY-plane sectioned into 2π -squares, as illustrated in Fig. A.1. Clearly, $F(x,y)$ is *identical* in each 2π -square and therefore periodic in two dimensions. A double Fourier series provides the values of $F(x,y)$ at each point in the 2π -square and thereby interently also on the OA line, i.e. the double Fourier series for the pulse width modulated pulse train is simply obtained by the substitution given in (27). The general expression of the double Fourier series is given by [2] :

$$\begin{aligned} F(x, y) &= \frac{1}{2} A_{00} \\ &+ \sum_{n=1}^{\infty} [A_{0n} \cos(ny) + B_{0n} \sin(ny)] \\ &+ \sum_{m=1}^{\infty} [A_{m0} \cos(mx) + B_{m0} \sin(my)] \\ &+ \sum_{m=1}^{\infty} \sum_{n=\pm 1}^{\pm \infty} [A_{mn} \cos(mx + ny) + B_{mn} \sin(mx + ny)] \end{aligned} \quad (28)$$

The Fourier coefficients are most conveniently expressed in complex form:

$$A_{mn} + jB_{mn} = \frac{1}{2\pi^2} \int_0^{2\pi} \int_0^{2\pi} F(x, y) e^{j(mx+ny)} dx dy \quad (29)$$

Since the three dimensional surface $F(x,y)$ is assumed constant, the double integral above is rather simple to solve:

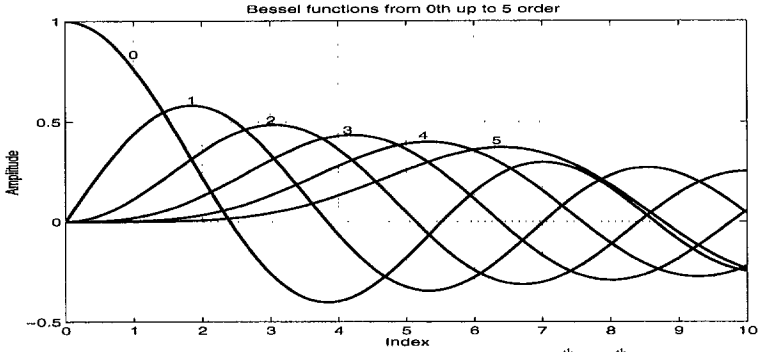


Figure A.2 Bessel functions of the first kind from 0th to 5th order.

$$\begin{aligned}
 A_{mn} + jB_{mn} &= \frac{1}{2\pi^2} \int_0^{2\pi} \int_0^{2\pi} F(x, y) e^{j(mx+ny)} dx dy \\
 &= -\frac{j}{2\pi^2 m} \int_0^{2\pi} (e^{j(m2\pi k + mM\pi \cos y + ny)} - e^{jny}) dy \\
 &= -\frac{j}{2\pi^2 m} e^{jm2\pi k} \int_0^{2\pi} e^{jmM\pi \cos y} \cdot e^{jny} dy \quad (m, n \neq 0) \\
 &= -\frac{j}{\pi m} e^{j(m2\pi k + n\frac{\pi}{2})} J_n(mM\pi) \quad (m, n \neq 0) \\
 &\quad \updownarrow \\
 A_{mn} &= \frac{j}{\pi m} \sin(m2\pi k + n\frac{\pi}{2}) J_n(mM\pi) \quad (m, n \neq 0) \\
 B_{mn} &= -\frac{j}{\pi m} \cos(m2\pi k + n\frac{\pi}{2}) J_n(mM\pi) \quad (m, n \neq 0)
 \end{aligned} \tag{30}$$

Evaluation of (30) at the special cases where either m or n is 0 is straightforward. By inserting the resulting coefficients in (28) the following double Fourier series arrive:

$$\begin{aligned}
 \tilde{F}_{NADS}(t) &= k + \frac{M}{2} \cos(y) \\
 &+ \sum_{m=1}^{\infty} \frac{\sin(mx)}{m\pi} - \sum_{m=1}^{\infty} \frac{J_0(m\pi M)}{m\pi} \sin(mx - 2m\pi k) \\
 &- \sum_{m=1}^{\infty} \sum_{n=\pm 1}^{\infty} \frac{J_n(m\pi M)}{m\pi} \sin(mx + ny - 2m\pi k - \frac{n\pi}{2})
 \end{aligned} \tag{31}$$

Setting $k = 0.5$ and by multiplying the series by a factor of 2 (corresponding to a total pulse height of 2) and after removing the DC component, the series is reduced to :

$$\begin{aligned}
F_{NADS}(t) &= M \cos(y) \\
&+ 2 \left(\sum_{m=1}^{\infty} \frac{\sin(mx)}{m\pi} - \sum_{m=1}^{\infty} \frac{J_0(m\pi M)}{m\pi} \sin(mx - m\pi) \right) \\
&- 2 \sum_{m=1n=\pm 1}^{\infty} \sum_{m=1}^{\infty} \frac{J_n(m\pi M)}{m\pi} \sin(mx + ny - m\pi - \frac{n\pi}{2}) \\
&\Downarrow
\end{aligned} \tag{32}$$

$$\begin{aligned}
F_{NADS}(t) &= M \cos(y) \\
&+ 2 \sum_{m=1}^{\infty} \frac{1 - J_0(m\pi M) \cos(m\pi)}{m\pi} \sin(mx) \\
&- 2 \sum_{m=1n=\pm 1}^{\infty} \sum_{m=1}^{\infty} \frac{J_n(m\pi M)}{m\pi} \sin(mx + ny - m\pi - \frac{n\pi}{2})
\end{aligned}$$

The series for all other modulation schemes can in principle be generated by a similar approach. Several modulation schemes have been synthesized in the literature. However, the alternative superposition approach used in the paper to derive the other expressions is considerably simpler and to be recommended where usable.

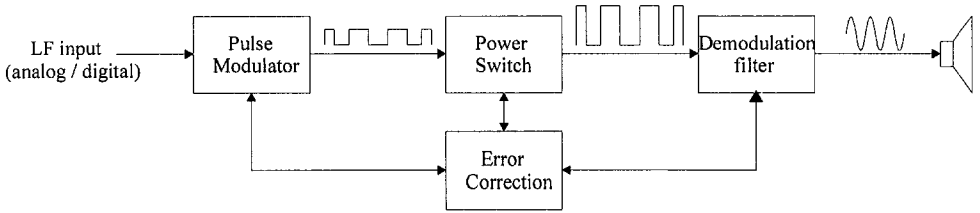


Fig. 1 Basic elements of a switching power amplifier system with analog or digital input.

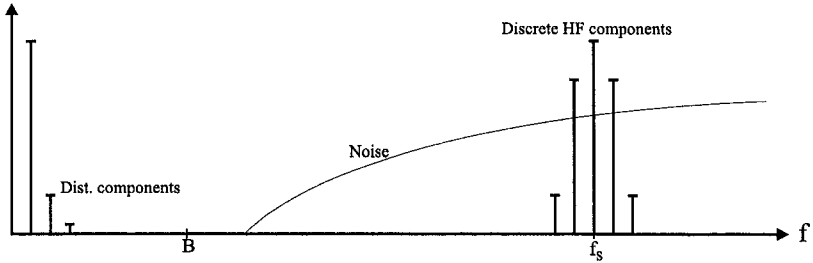


Fig. 2 General pulse modulator output characteristics. The HF spectrum may be discrete, stochastic (noise) or a combination of both.

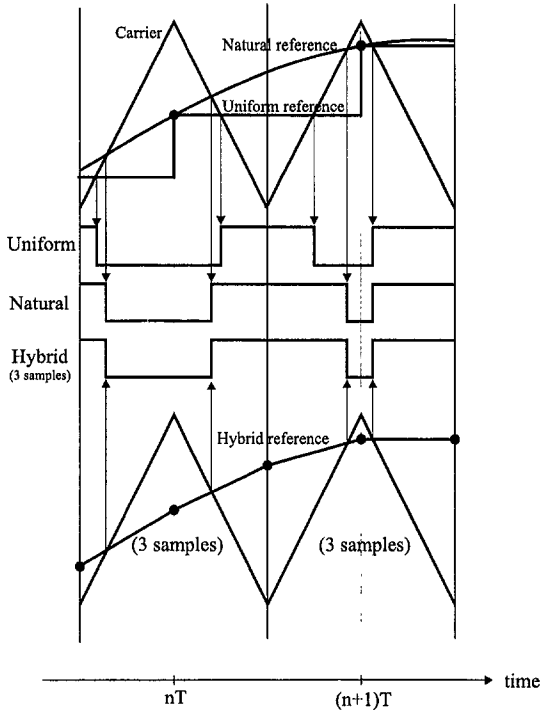


Fig. 3 Basic pulse width modulation schemes.

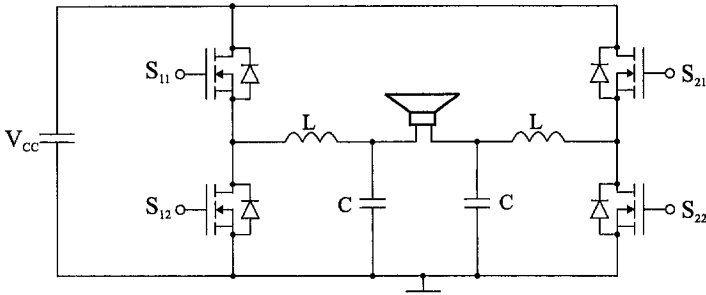


Fig. 4 Bridge power stage, which can realize all the considered modulation schemes.

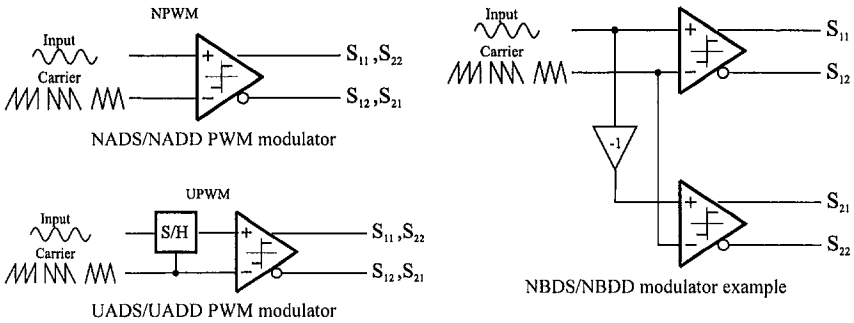


Fig. 5 Examples of modulator structures.

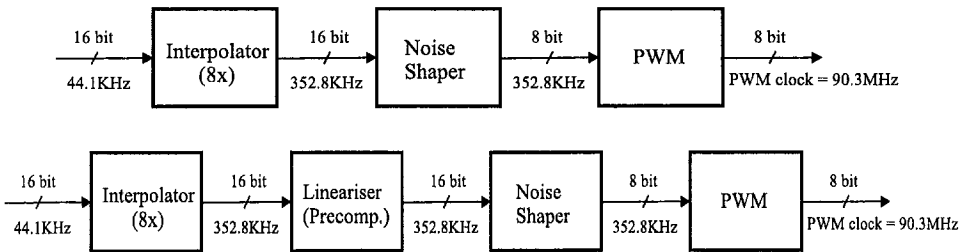


Fig. 6 Practical implementation of digital UPWM and LPWM modulators. Noise shaping is required in order to obtain reasonable PWM counter clock speeds.

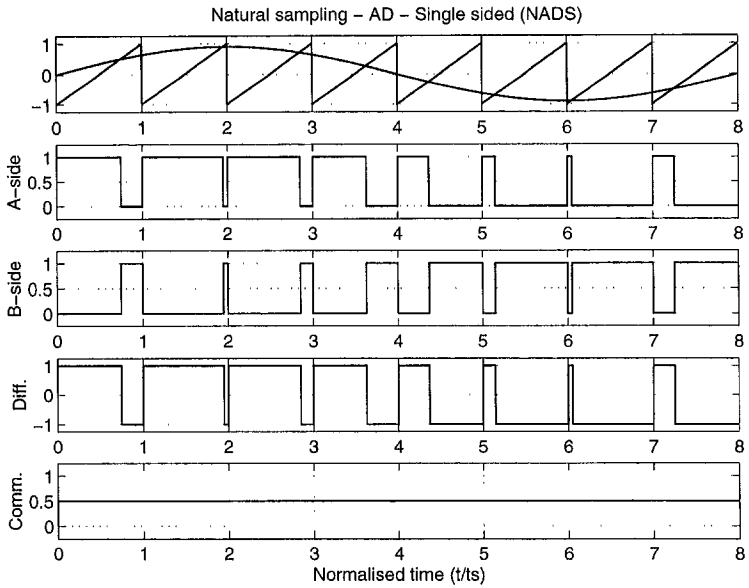


Fig. 7 Time domain waveforms for NADS

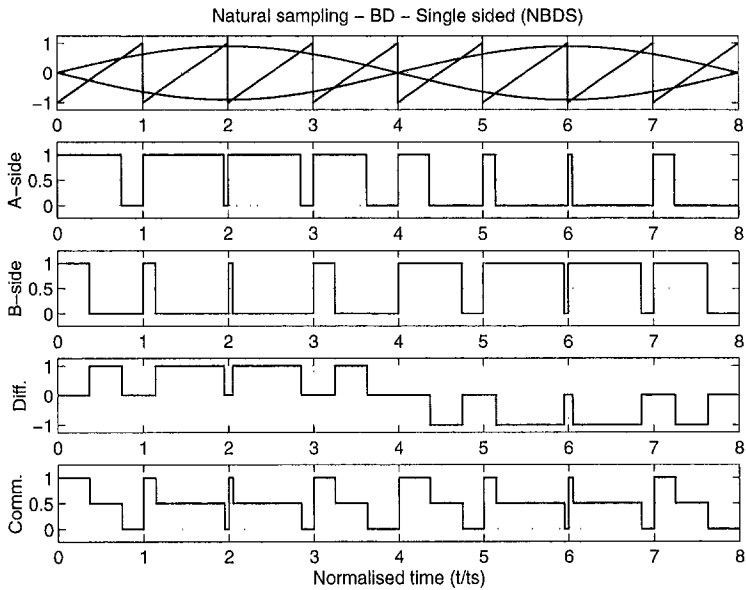


Fig. 8 Time domain waveforms for NBDS.

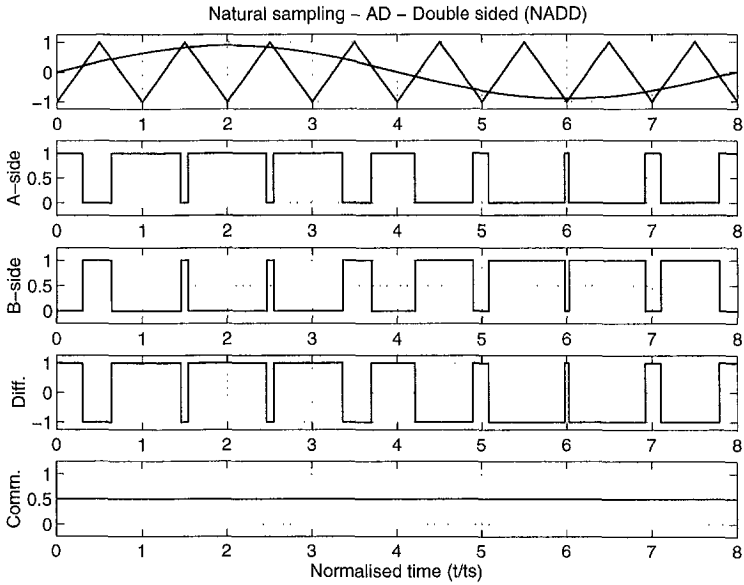


Fig. 9 Time domain waveforms for NADD.

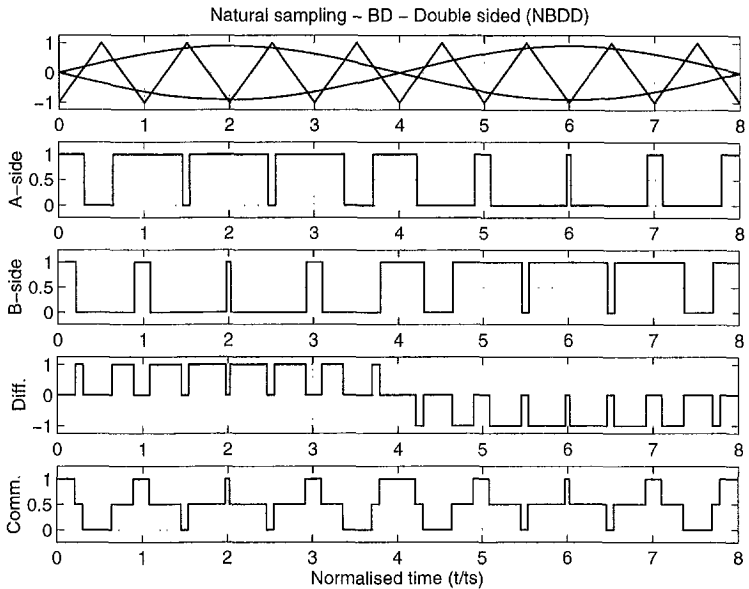


Fig. 10 Time domain waveforms for NBDD.

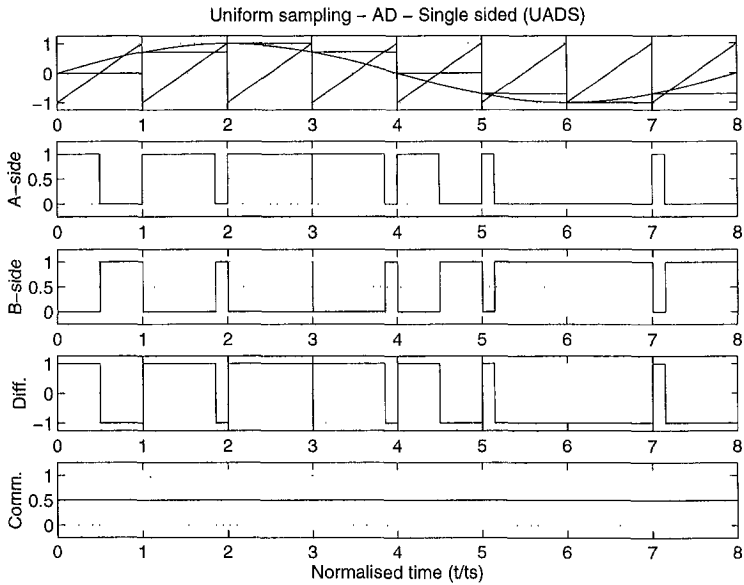


Fig. 11 Time domain waveforms for UADS.

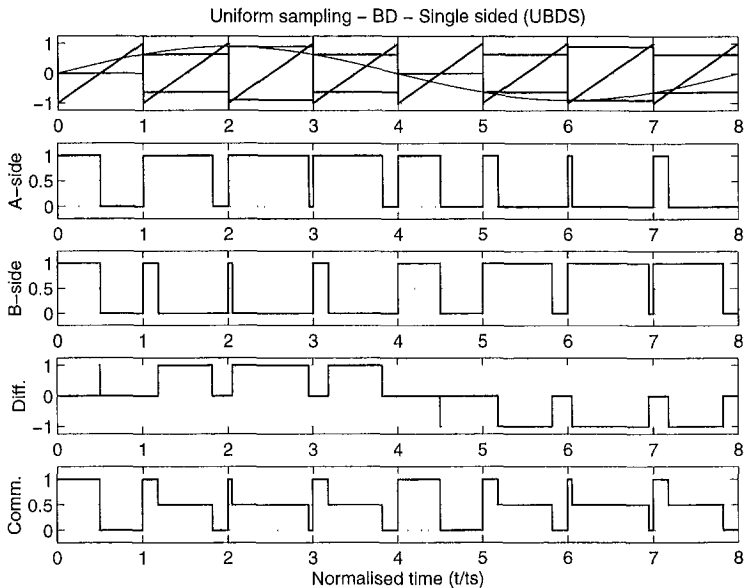


Fig. 12 Time domain waveforms for UBDS.

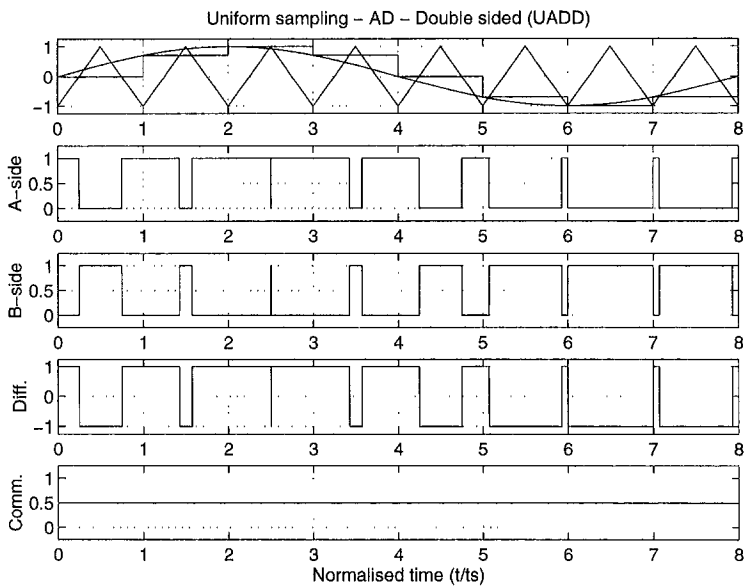


Fig. 13 Time domain waveforms for UADD.

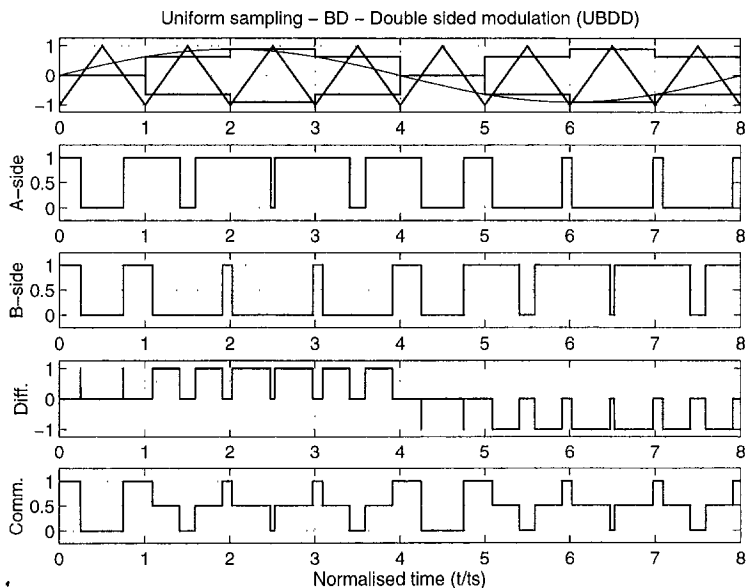


Fig. 14 Time domain waveforms for UBDD.

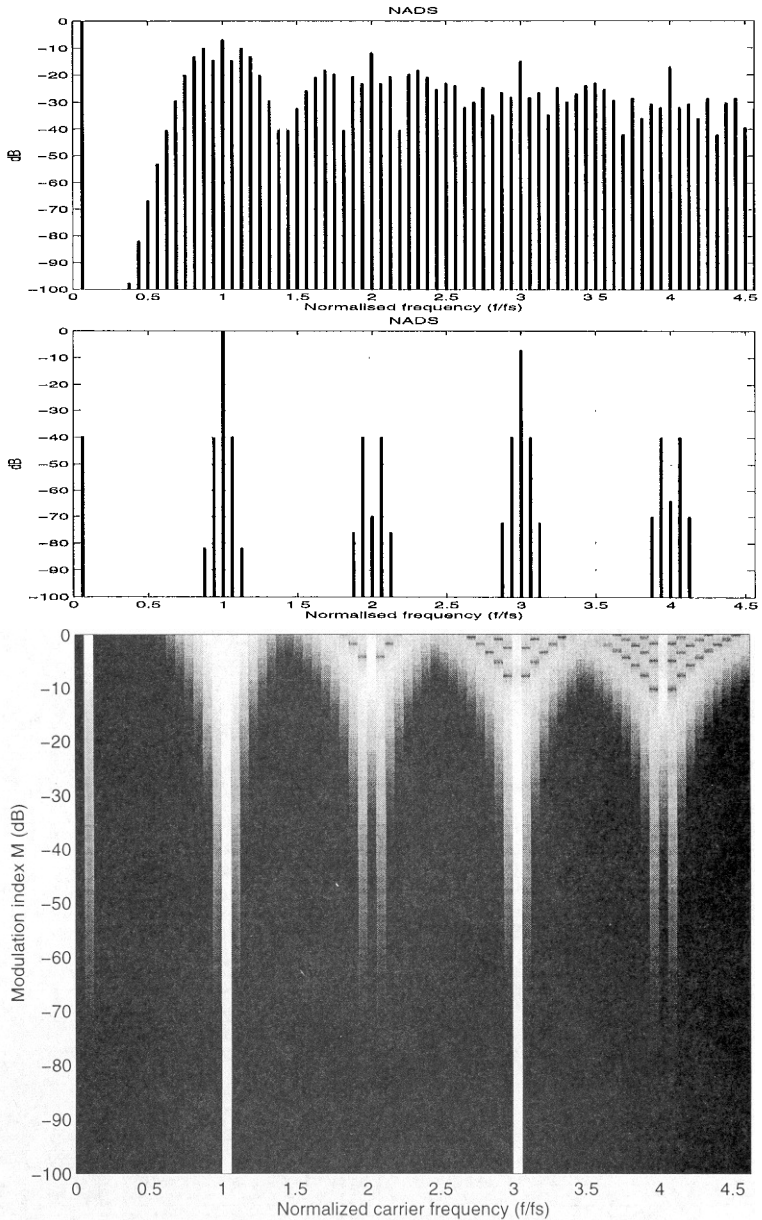


Fig. 15 Frequency domain characteristics for NADS, illustrated the harmonic spectrum and a HES-plot with M varying from -100dB to 0dB (full scale). $q=1/16$.

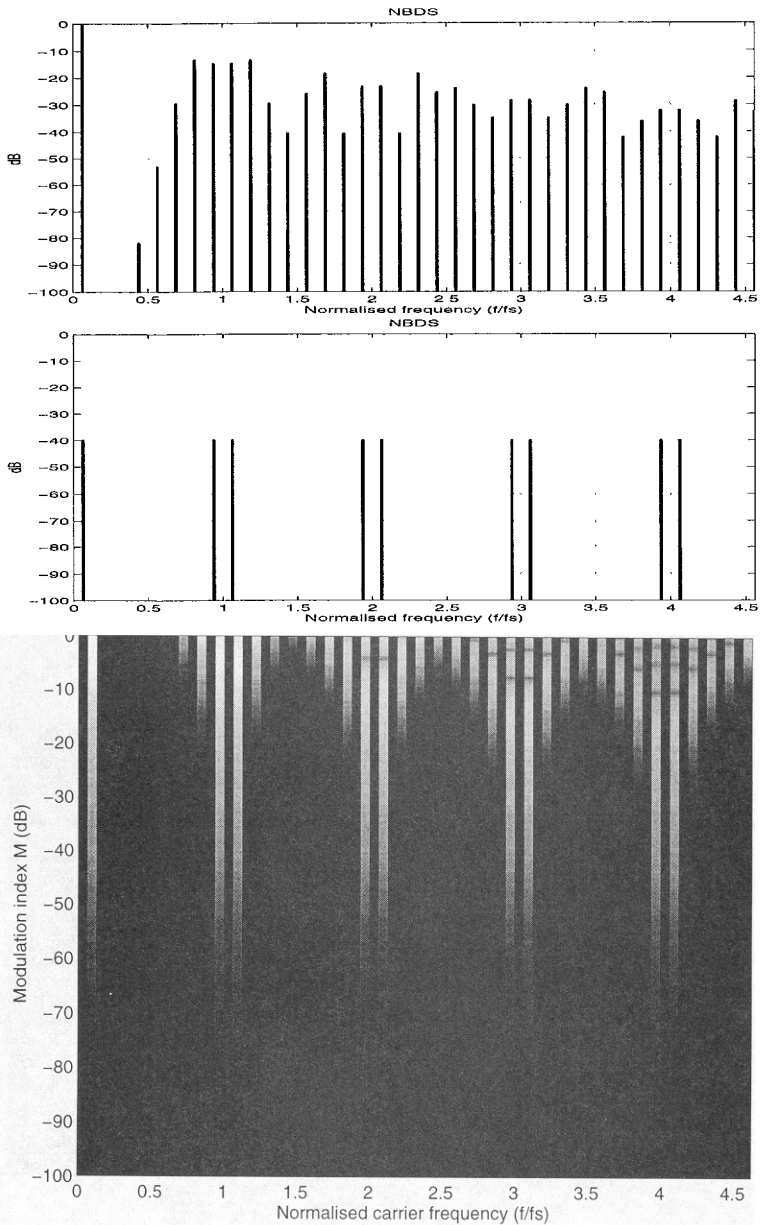


Fig. 16 Frequency domain characteristics for NBDS, illustrated the harmonic spectrum and a HES-plot with M varying from -100dB to 0dB (full scale). $q=1/16$.

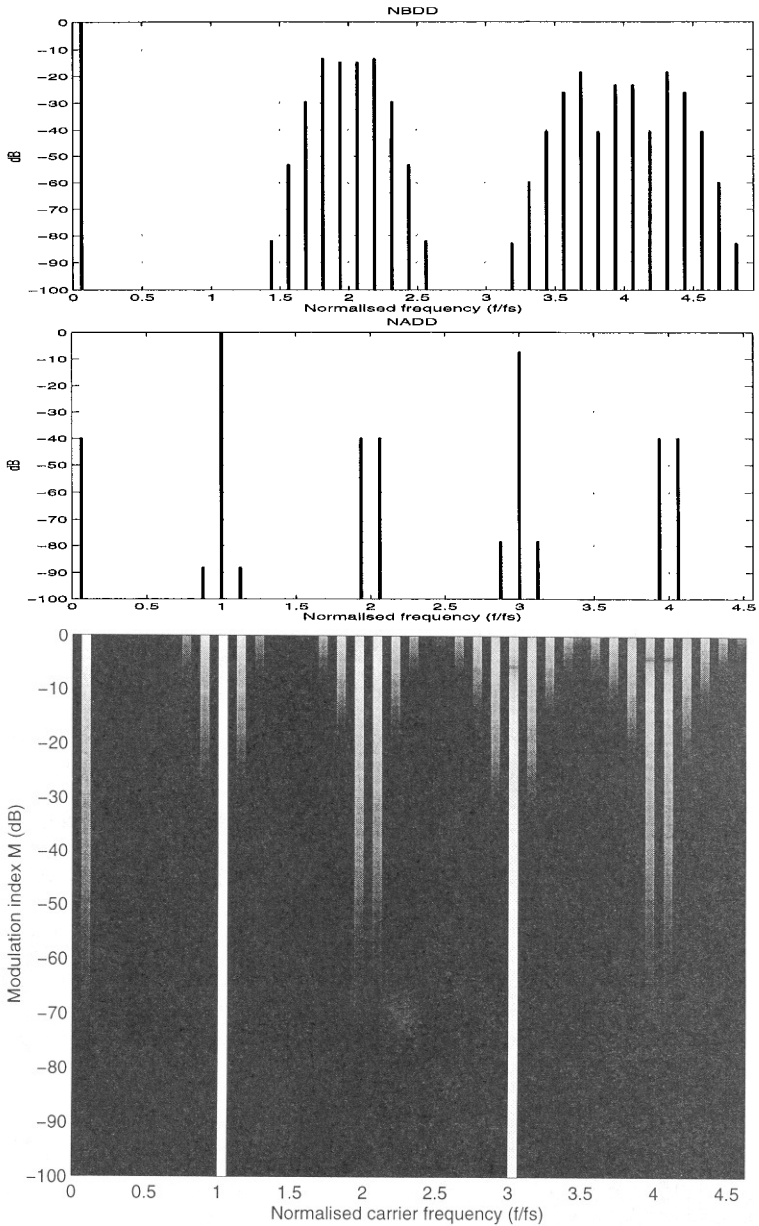


Fig. 17 Frequency domain characteristics for NADD, illustrated the harmonic spectrum and a HES-plot with M varying from -100dB to 0dB (full scale). $q=1/16$.

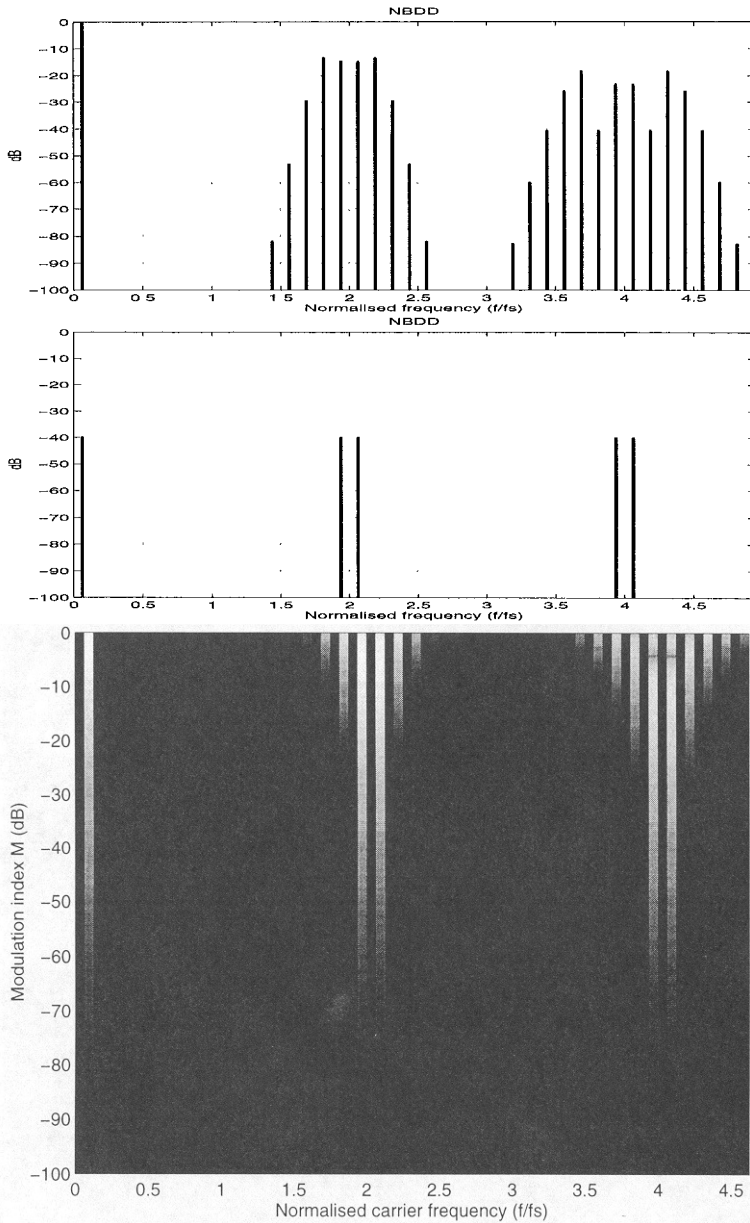


Fig. 18 Frequency domain characteristics for NBDD, illustrated the harmonic spectrum and a HES-plot with M varying from -100dB to 0dB (full scale). $q=1/16$.

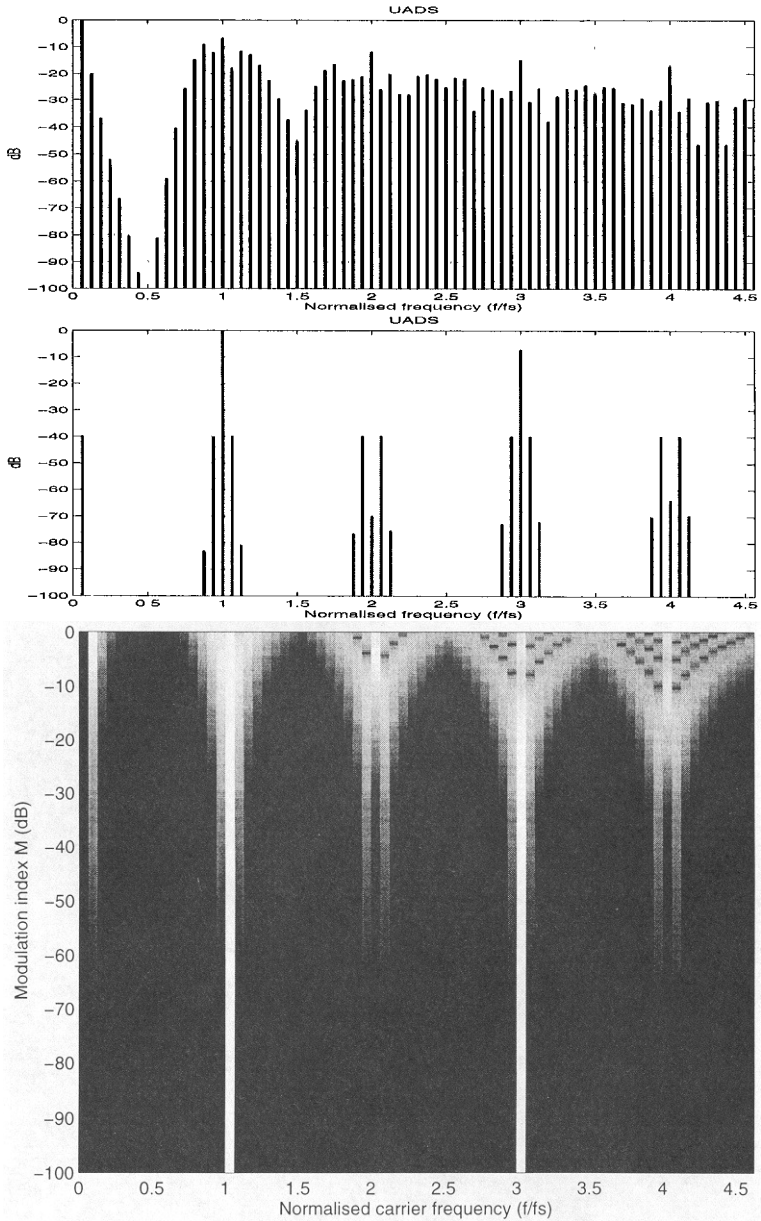


Fig. 19 Frequency domain characteristics for UADS, illustrated the harmonic spectrum and a HES-plot with M varying from -100dB to 0dB (full scale). $q=1/16$.

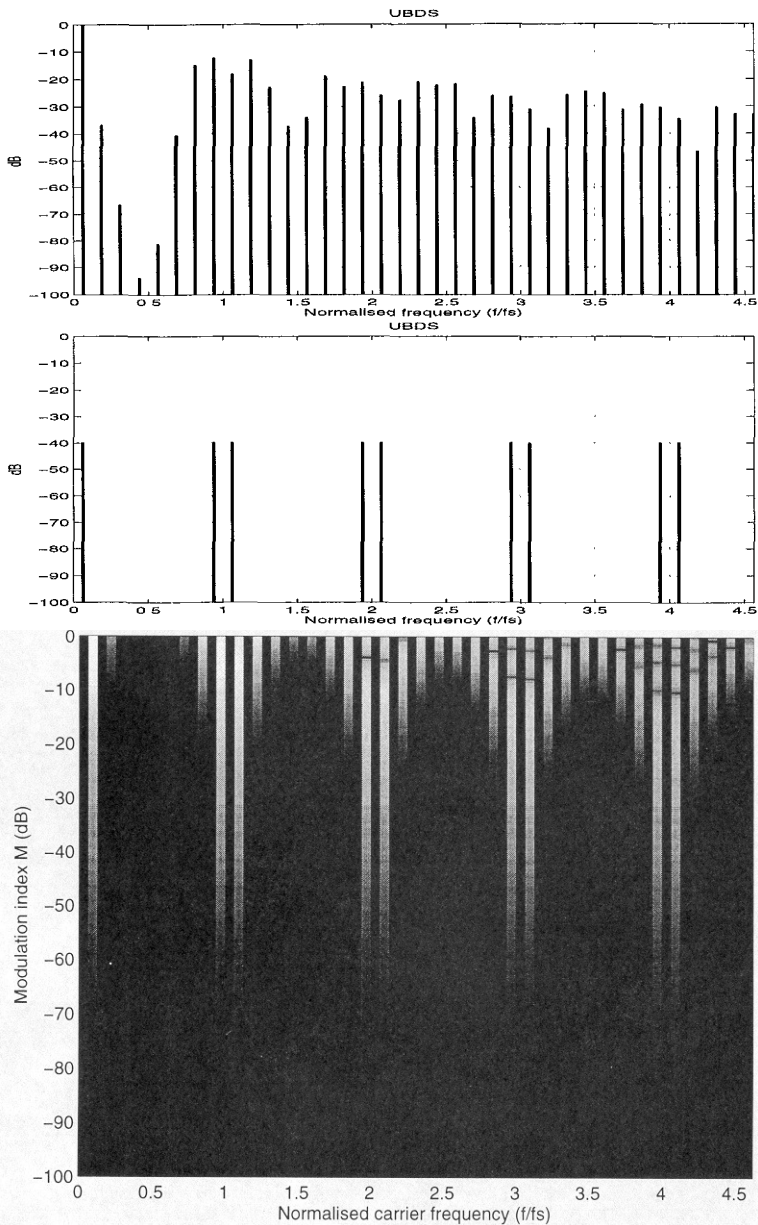


Fig. 20 Frequency domain characteristics for UBDS, illustrated the harmonic spectrum and a HES-plot with M varying from -100dB to 0dB (full scale). $q=1/16$.

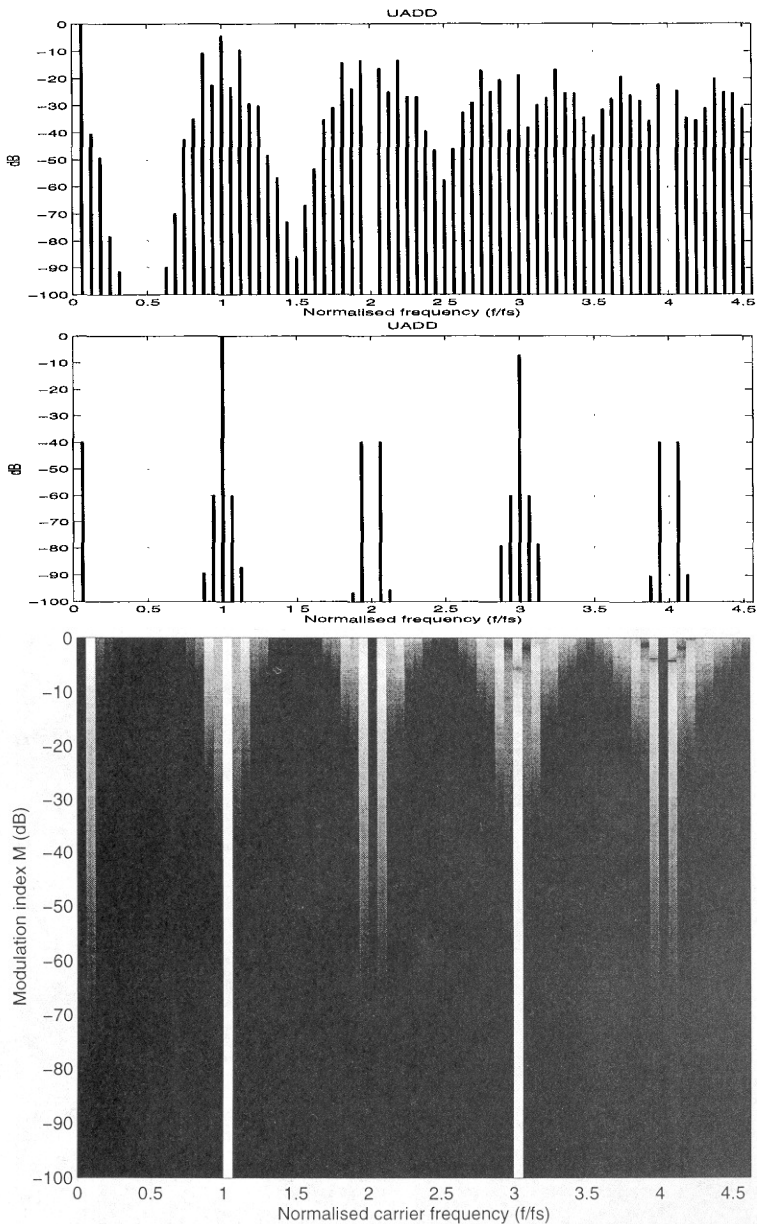


Fig. 21 Frequency domain characteristics for NADD, illustrated the harmonic spectrum and a HES-plot with M varying from -100dB to 0dB (full scale). $q=1/16$.

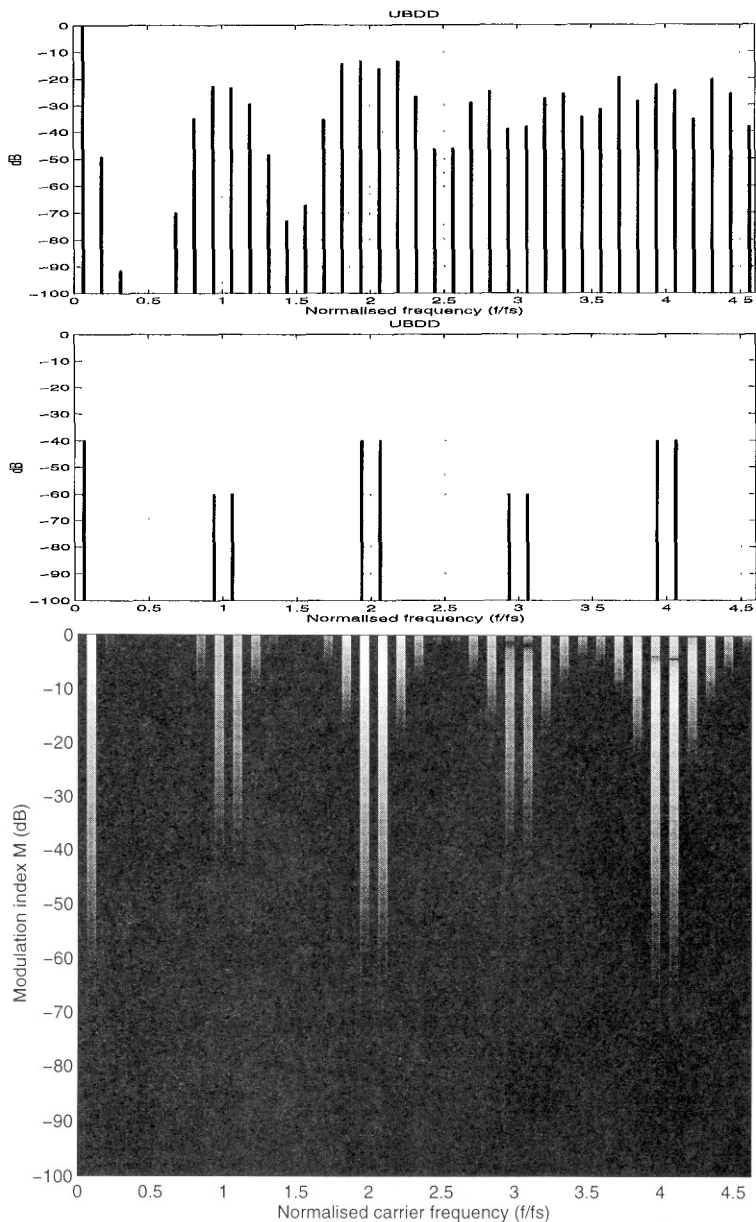


Fig. 22 Frequency domain characteristics for UBDD, illustrated the harmonic spectrum and a HES-plot with M varying from -100dB to 0dB (full scale). $q=1/16$.

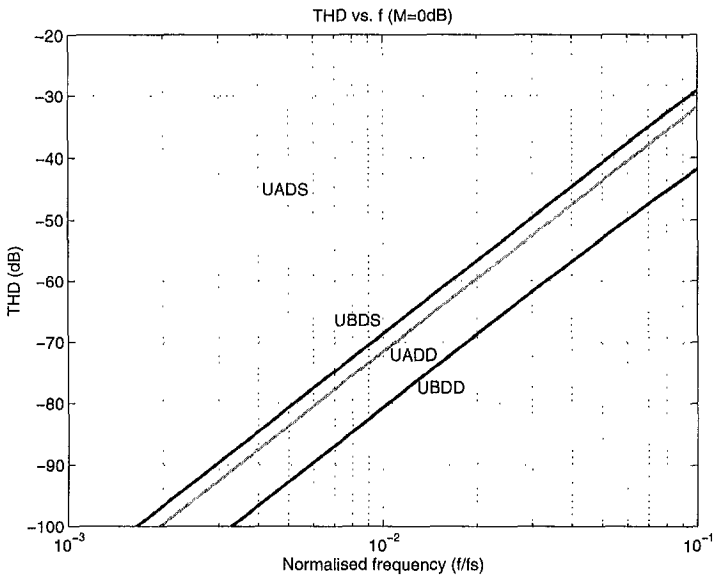


Fig. 23 UPWM THD vs. q.

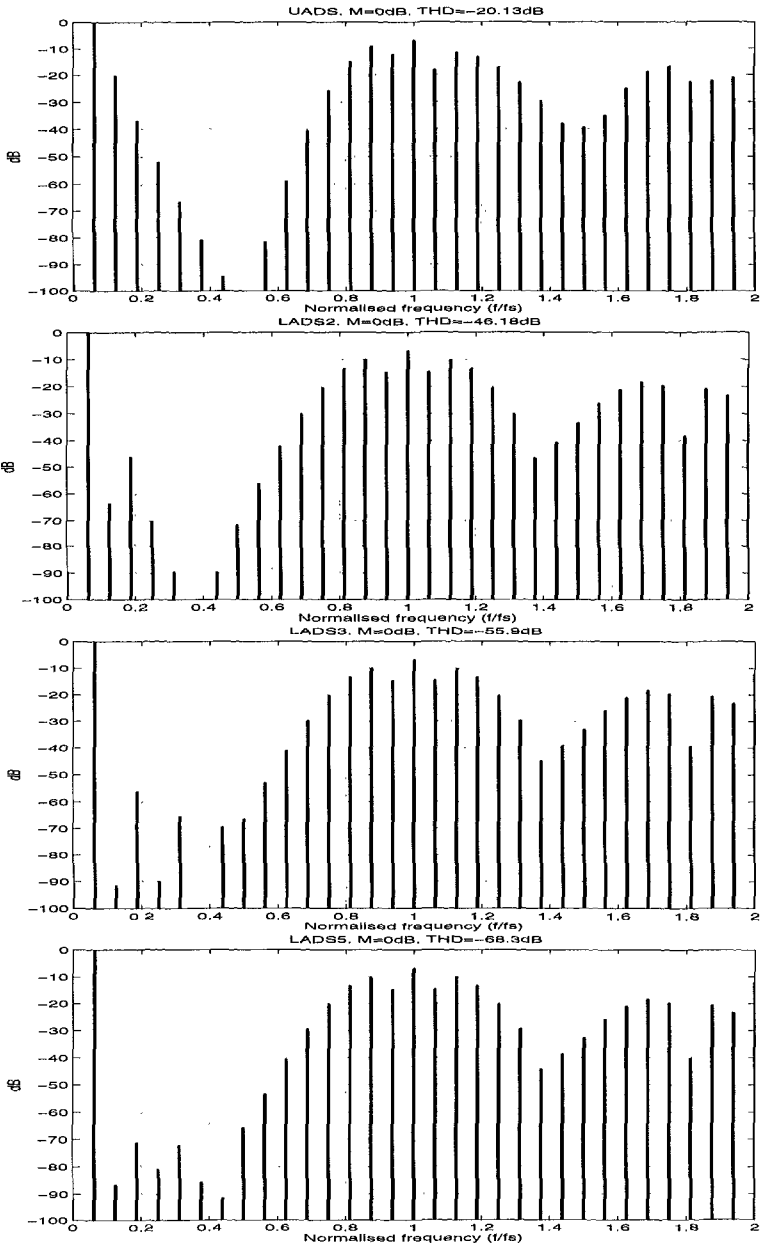


Fig. 24 Spectral characteristics for LADS for $s \in \{1, 2, 3, 5\}$. $q = 1/16$. $M=0\text{dB}$.

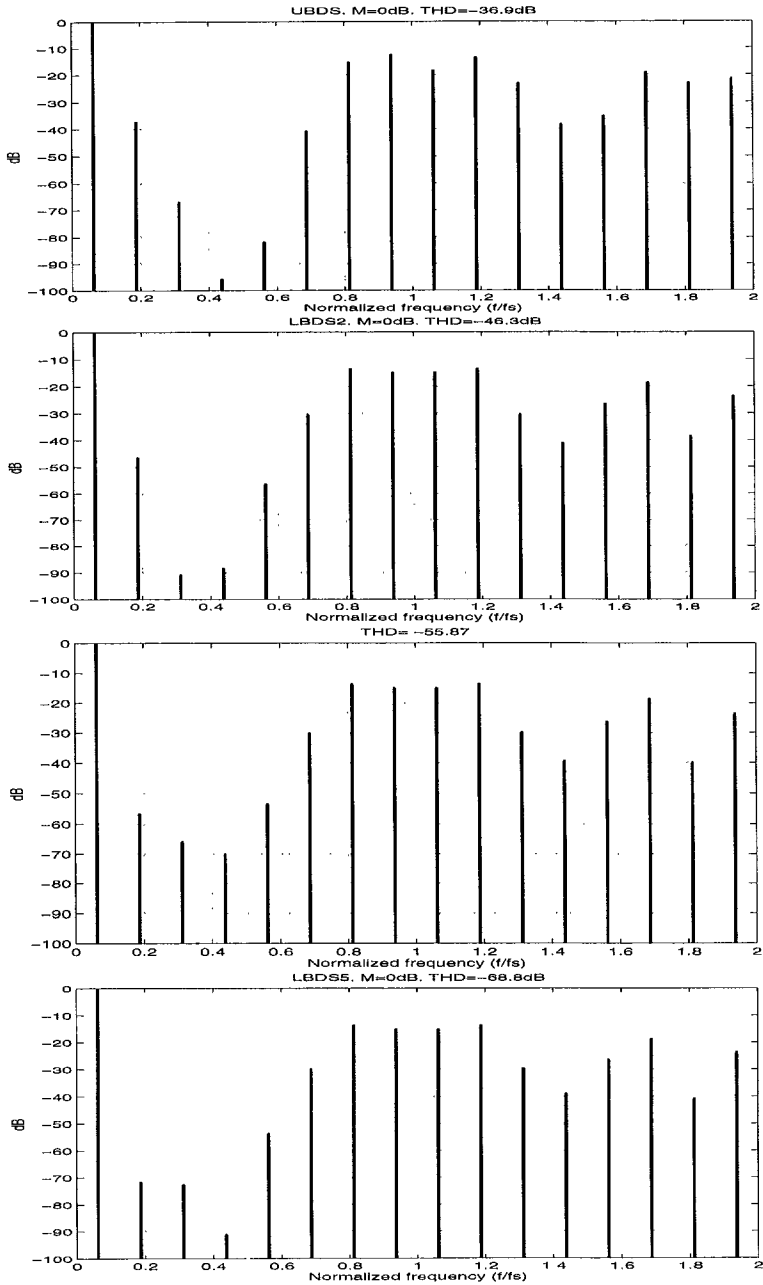


Fig. 25 Spectral characteristics for LBDS for $s \in \{1, 2, 3, 5\}$. $q = 1/16$. $M = 0\text{dB}$.

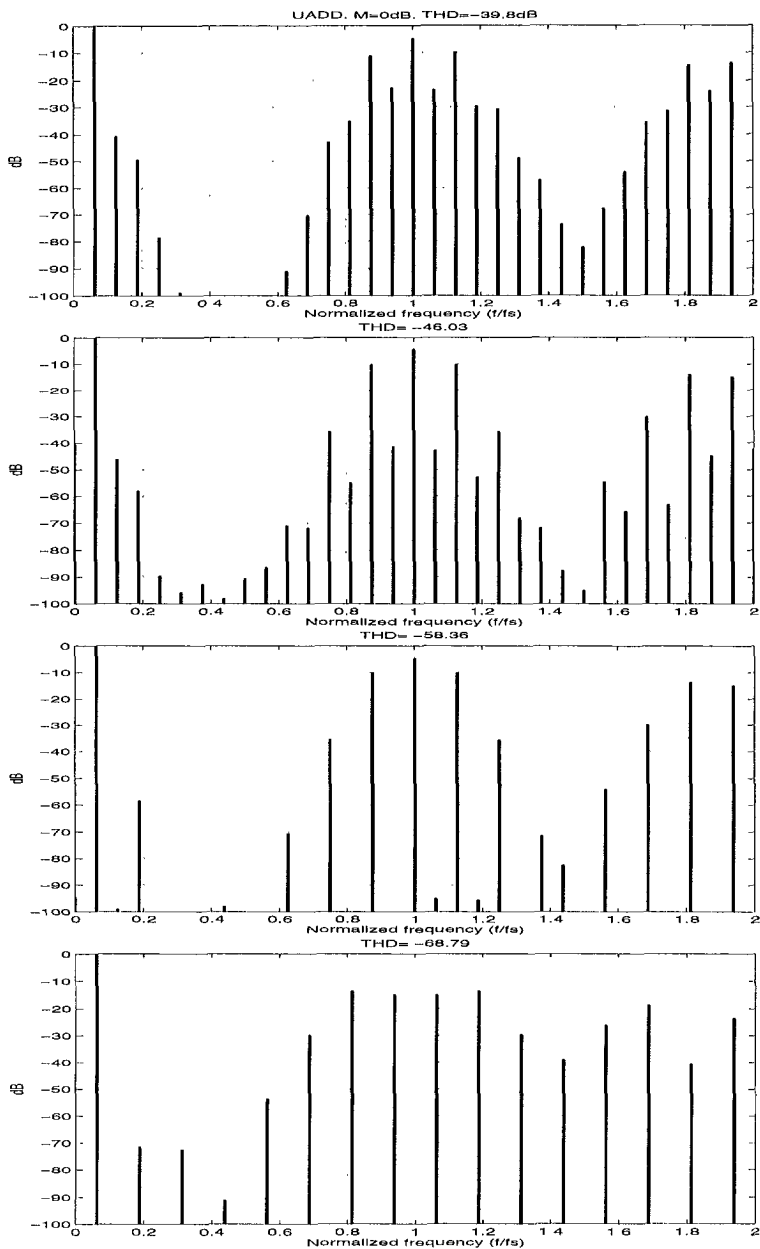


Fig. 26 Spectral characteristics for LADD for $s \in \{1, 2, 3, 5\}$. $q = 1/16$. $M=0\text{dB}$.

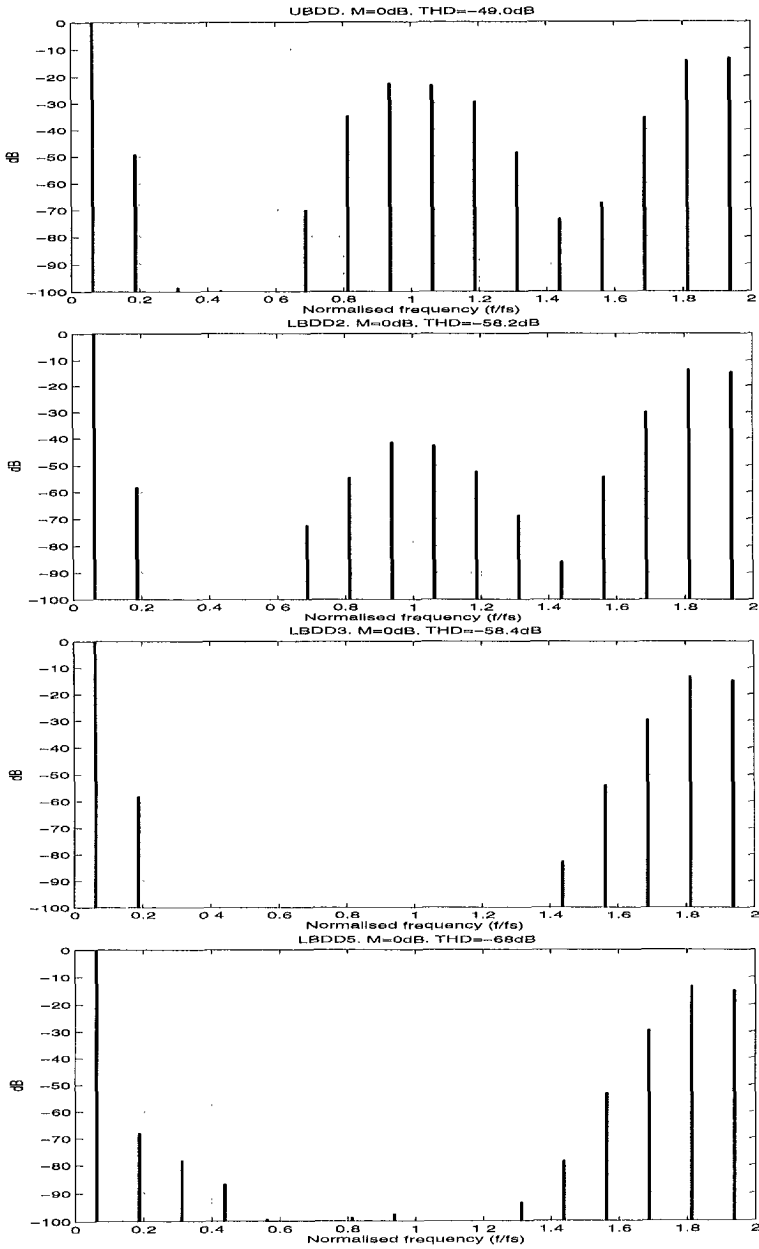


Fig. 27 Spectral characteristics for LBDD for $s \in \{1, 2, 3, 5\}$. $q = 1/16$. $M=0$ dB.

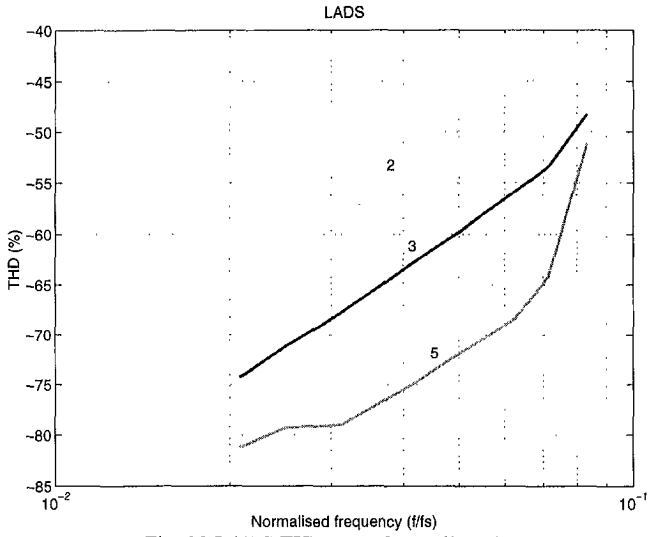


Fig. 28 LADS THD vs. q for $s \in \{2,3,5\}$.

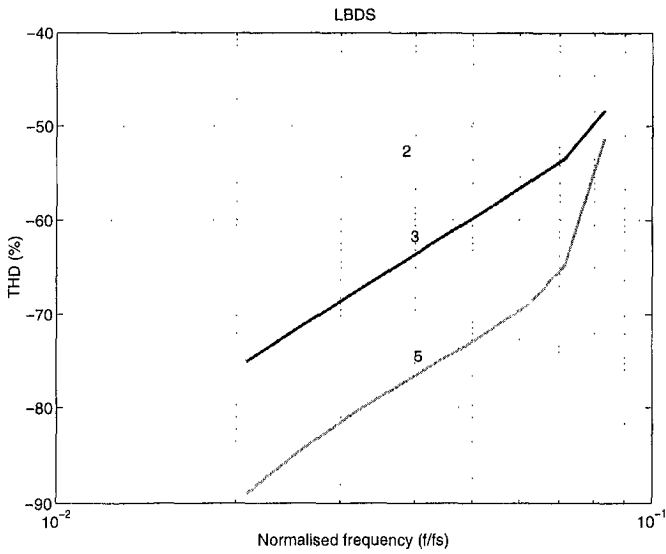


Fig. 29 LBDS THD vs. q for $s \in \{2,3,5\}$.

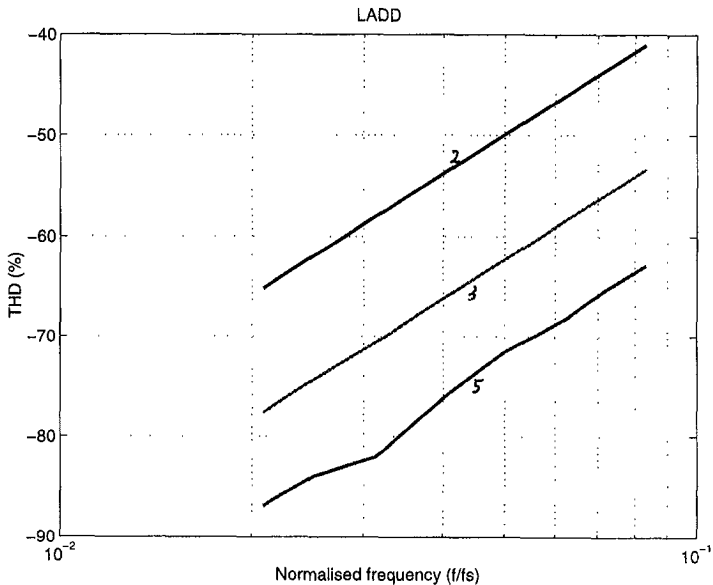


Fig. 30 LADD THD vs. q for $s \in \{2,3,5\}$.

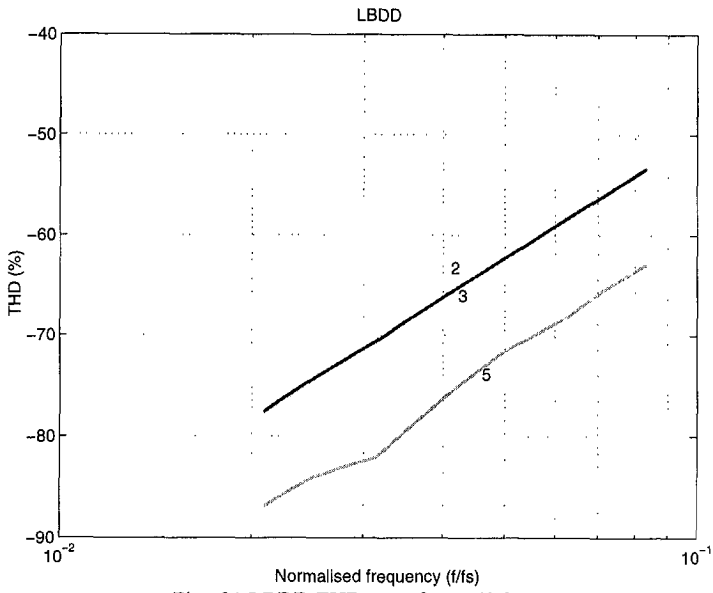


Fig. 31 LBDD THD vs. q for $s \in \{2,3,5\}$.

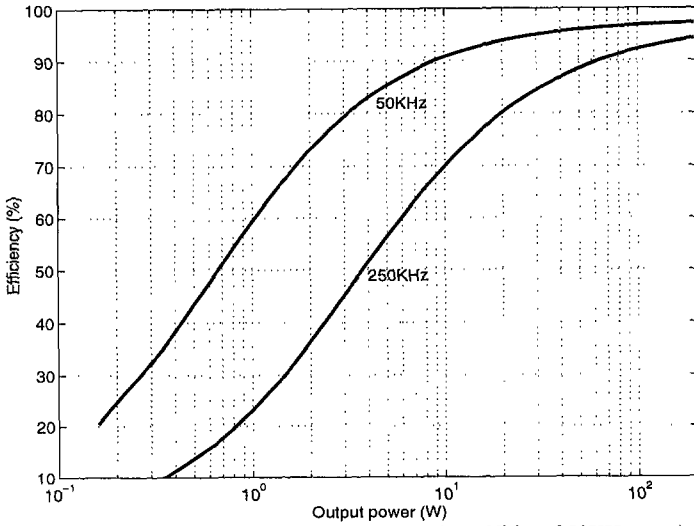


Fig.32 Power stage efficiency for 200W examples. With a 250KHz carrier frequency (20KHz bandwidth) the efficiency approaches 92%, and at 50KHz carrier frequency (4KHz bandwidth) 96% efficiency is obtained at higher output powers.

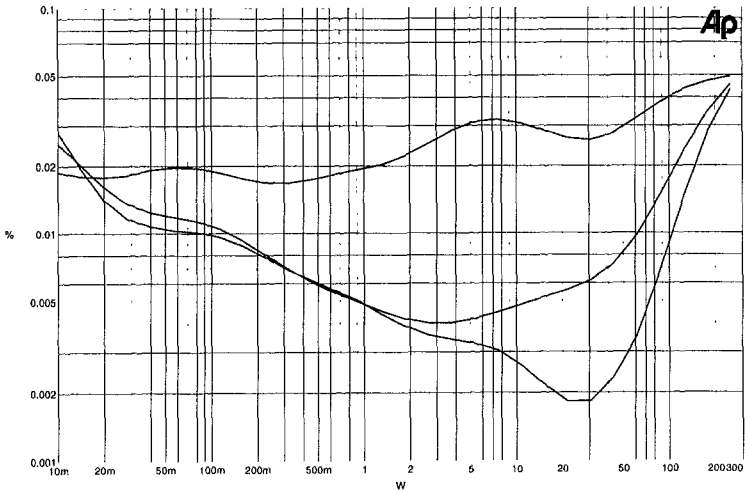


Fig 33 THD+N vs output power at 100Hz, 1KHz and 10KHz. Note, that THD+N is measured over a very broad power range from 10mW to 250W.

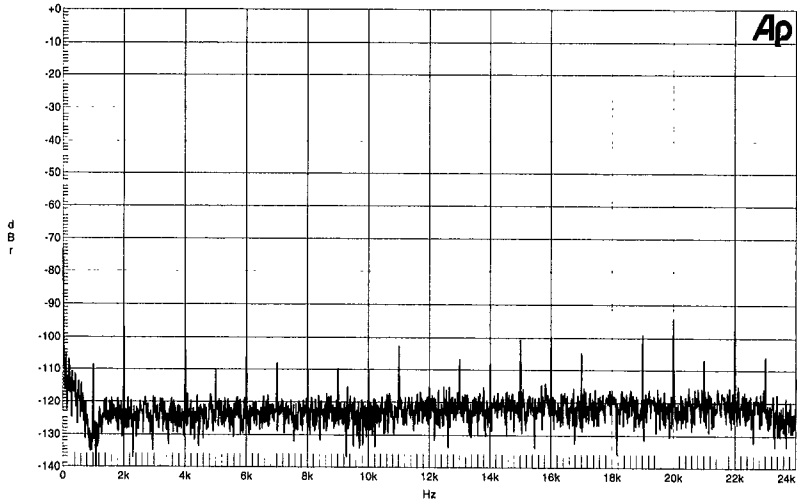


Fig 34 Harmonic residue at 1KHz/1W (re 1W). Note, that all harmonics are damped at least 95dB. The 2. harmonic distortion is thus 0.0015%.

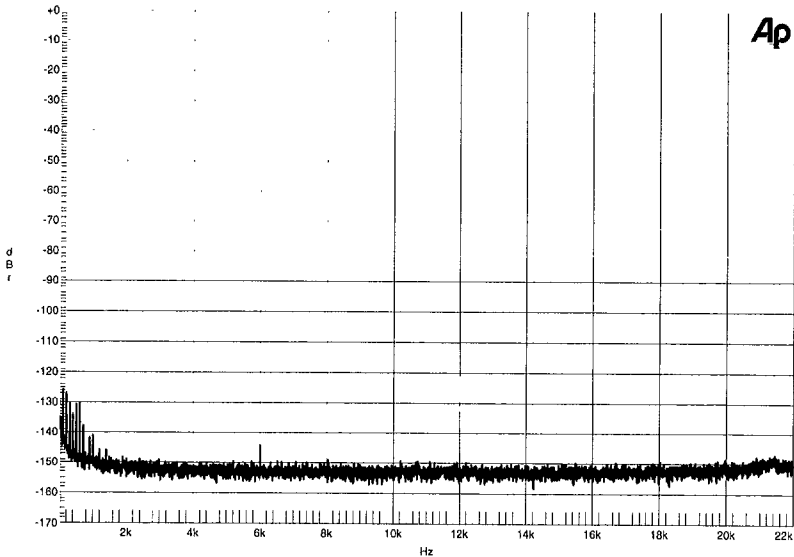


Fig. 35 The well distributed amplifier noise at idle with terminated input (re full scale). The noise floor corresponds to an audio band RMS noise level of $50\mu\text{V}$, corresponding to an unweighted dynamic range of 118dB.

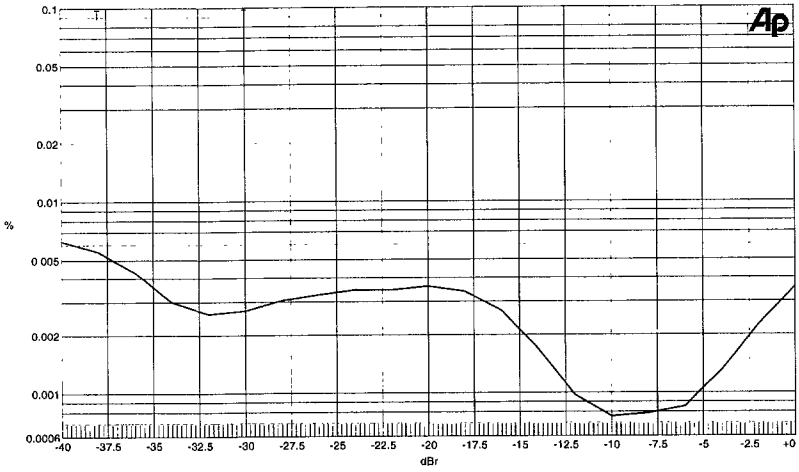


Fig. 36 Two tone intermodulation distortion (CCIF) vs. output level. The two tones are 19KHz and 20KHz.